國立台灣大學電機資訊學院電機工程學研究所

博士論文

Graduate Institute of Electrical Engineering

College of Electrical Engineering and Computer Science

National Taiwan University

Doctoral Dissertation

穴蝕效應及輻射力在超音波血栓溶解及藥物傳輸所扮演的角色

Roles of Cavitation and Radiation Force in Sono-thrombolysis and Drug Delivery

莊岳勳

Yueh-Hsun Chuang

指導教授: 李百祺 博士

Advisor: Pai-Chi Li, Ph.D.

中華民國 102 年 7 月
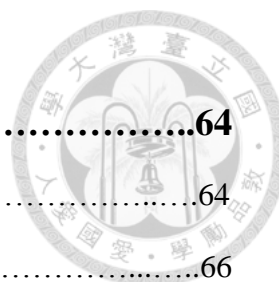
July 2013

Table of Contents:

Abstract

Acoustic cavitation has been studied in application of thrombolysis. Radiation force induces gaps between endothelium and enhances the delivery of therapeutic substances. First, we evaluated the effects of cavitation, microbubbles (MBs), and streptokinase on thrombolysis. We found that temperature rise cannot fully explained enzymatic sonothrombolysis and the differential inertial cavitation dose is a good indicator. Second, we examined the efficacy of using radiation forces to localize and enhance the targeting of MBs in cavitation-induced sonothrombolysis. Our observations confirm that radiation forces help MBs to distribute into a clot (as does cavitation). Combining radiation forces with cavitation would provide additional thrombolysis effects relative to cavitation alone. A local delivery method based on radiation forces has the potential to improve the safety and efficacy of sonothrombolysis. Third, we hypothesized that albumin MBs can be used for drug delivery to breast cancer cells without antibody conjugation for specific targeting. We also studied the possible roles of TGF-β_1 and a radiation force in the behavior of cells and albumin MBs. The results show that albumin MBs can enter breast cancer cells and remain therein for at least 24 hours, even in the presence of paclitaxel loading. Applying radiation force further increased the percentage. This process could be blocked by TGF-β_1, even with subsequent exposure to the radiation force. From these results we conclude that TGF-β_1 receptors are involved in endocytosis of albumin MBs entering breast cancer cells. The albumin MBs without antibody conjugation can be a useful method of drug delivery. The entire study we presented here demonstrates that radiation force and cavitation play different roles and are important in thrombolysis and drug delivery.
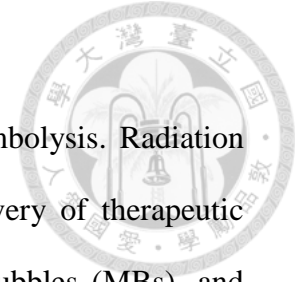
中文摘要

　　超音波穴蝕效應已經有很多研究嘗試運用在血栓溶解上，超音波輻射力可以使血管內皮細胞間隙變寬，及促進治療物質的傳送。首先，我們評估了結合穴蝕效應、微氣泡及鏈激酶對於血栓溶解的效應。我們發現溫度上升不能完全解釋酵素引發的血栓溶解效應，以及差異性惰性穴蝕效應劑量可以是一個有效的血栓溶解指標。第二部分則是對於穴蝕效應引發的血栓溶解效應，我們檢視了利用施加超音波輻射力對於聚集及標定微氣泡所產生的效果。我們的觀察也確定了輻射力可以幫助微氣泡分布到血栓內部，穴蝕效應也同樣可以。結合輻射力及穴蝕效應相對應於單純施加穴蝕效應，可以提供額外的血栓溶解效果。超音波輻射力所提供的局部傳遞效果，有潛力可以用來提高超音波血栓溶解的安全性及效果。第三部分我們假設了白蛋白微氣泡在不使用抗體作為專一性標定的情況下，可以針對乳癌細胞進行藥物傳送。我們同時也研究了超音波輻射力以及轉化生長因子 TGF-β1，對於白蛋白微氣泡跟細胞之間互動的可能扮演角色。結果顯示白蛋白微氣泡可以進入乳癌細胞而且存活超過 24 小時，即使氣泡帶有太平洋紫杉醇藥物也可以。施加輻射力更可以增加這個現象的百分比。然而這個現象可以被轉化生長因子 TGF-β1 阻斷，即使後續施加輻射力也是如此。由此我們得到的結論是轉化生長因子 TGF-β1 的接受器應該有參與白蛋白微氣泡進入乳癌細胞的細胞吞噬作用。另外，白蛋白微氣泡在沒有抗體接合來輔助標定的情況下，依然可以是一個傳遞藥物的有效方法。整體來說，我們在此呈現的研究，主要展現了超音波輻射力及穴蝕效應對於血栓溶解及藥物傳遞上，扮演了不同且重要的角色。

Chapter 1

Introduction

Ultrasound (US) imaging has been used clinically as an effective diagnostic tool since the 1960s [1-3]. It is a noninvasive medical examination that helps physicians diagnose and treat medical conditions. The advantages include real time imaging, non-invasive or minimally invasive, bedside availability, relatively cheaper than computed tomography and magnetic resonance imaging, and no radiation. However, there are some limitations in applications about medical ultrasound. First, the operation of ultrasound depends on operator's skill and experiences. Second, the display window and penetration depth are limited. Third, organs that contain air or bone are poorly visualized. Ultrasound can also be a way of treatment. Local heating by ultrasound for physical therapy, extracorporeal shock wave lithotripsy, and high intensity focused ultrasound are wellknown examples. Extensive work has been done in the past showing harmful biological responses of cells and tissues to ultrasound exposure including growth suppression, retarded protein synthesis, cytoplasmic vacuolation and disruption of intracellular components such as mitochondria, microtubules and endoplasmic reticulum [4]. Ultrasonic bioeffects can result from thermal and non-thermal mechanisms [3,5]. Both mechanisms are important and either may predominate, depending on the exposure conditions [6]. The thermal mechanism associated with the absorption of acoustic energy by the body and the generation of heat is reasonably well understood [7]. Non-thermal mechanisms are typically insignificant, unless a phenomenon known as cavitation occurs [8-12].

In recent years, lots of attention in research has been paid in acoustic cavitation. This can be described briefly as the growth and oscillation of MBs in response to a driving acoustic field. If the acoustic and medium conditions are conducive, the MBs

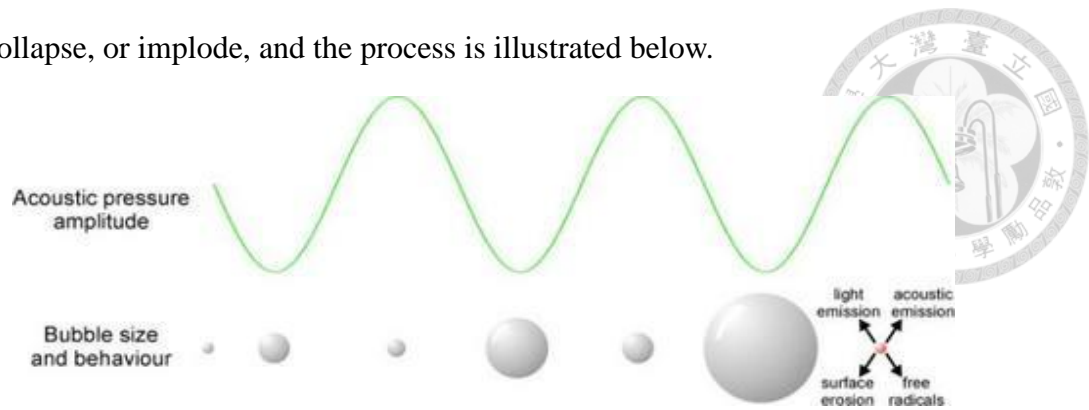can collapse, or implode, and the process is illustrated below.
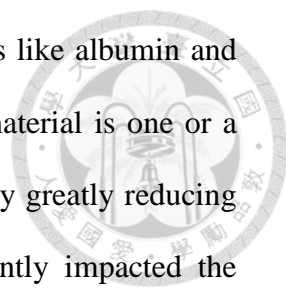
Figure 1. Bubble behavior under acoustic exposure.

A bubble initially at rest can grow during the rarefaction half-cycles of an applied acoustic field. Through rectified diffusion, gas and vapor are transported into the bubble, until it reaches a critical size and collapses. The bubble contents are compressed rapidly, resulting in extreme local conditions. Extreme conditions occur at the collapse phase, perhaps with temperatures up to 5000 °K and pressures of 1000 atmospheres. The cavitation process is more efficient with the presence in the liquid of small pockets of gas trapped in conical pits of solid impurities or covered with an organic or surface-active molecule, the so called nuclei. The gas inside bubbles provides another way of contrast relative to that of tissues in ultrasonography. As the quantity of nuclei in the liquid increases, lower energy is needed for cavitation inception. Bubbles can be either injected in some fluids or formed spontaneously due to the action of a pertinent source. For instance, there exist reports that sufficiently high amplitude ultrasound pulses cavitate the nucleation agents present in blood [13-15].

Until now, different kinds of MBs were developed and studied for their characteristics and applications. Contrast MBs are usually stabilized against dissolution and coalescence by the presence of additional materials at the gas-liquid interface [16-18]. In some cases, this material is an elastic solid shell that enhances stability by support-

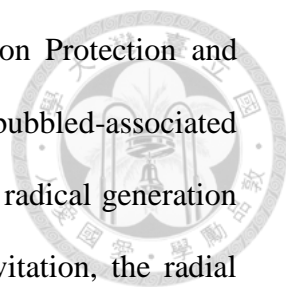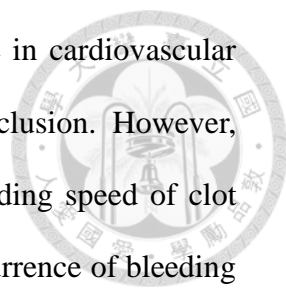ing a strain to counter the effect of surface tension. Shell materials like albumin and polymer are examples to meet this purpose. In other cases, this material is one or a combination of two or more surfactants, which promote stability by greatly reducing the surface tension at the interface. Lipid composition significantly impacted the acoustic dissolution rate, fragmentation propensity, and mechanism of excess lipid shedding [19]. Currently, some perfluorochemicals (PFCs) are being used as MB filling gases due to their low solubility in blood and high saturation vapor pressure. The amount of PFCs is controlled to impart sufficient vapor pressure to counter the sum of the Laplace pressure (surface tension) and arterial blood pressure. Both the constraining surface materials and insoluble filling gas of a contrast microbubble inhibit it to a certain degree from undergoing a swift expansion and, subsequently, a violent collapse that may occur to a free microbubble [17]. It is well-known that intense US causes the disappearance of contrast MBs [20-22], but the exact mechanism of destruction is only partially understood and little is known regarding the relationship between cavitation bioeffects and microbubble destruction. MBs like Albunex and Optison (Molecular Biosystems, Inc., San Diego, CA) consist of gas (air and PFCs, respectively) MBs encapsulated within a shell of human serum albumin. However, each contrast agent exhibits different responses to ultrasound pulses because of the unique properties of the MB surface materials and filling gases. Acoustic pressures causing MB destruction for one agent are usually not necessarily the same for another agent. This implies that the conditions for the safe use of one agent may lead to potentially hazardous bioeffects if the same conditions are applied to another agent. Therefore, it is imperative to identify the conditions for the safe use of each new contrast agent.

Acoustic cavitation has been studied by many investigators interested in US bio-
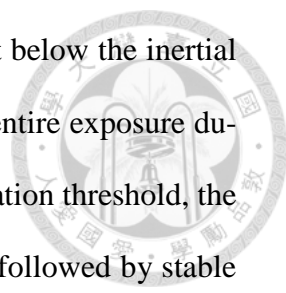
effects. In its 1983 report [23], the National Council on Radiation Protection and Measurements identified both stable cavitation processes such as bubbled-associated microstreaming [24] and inertial cavitation processes, such as free radical generation and microjetting, as possible mechanisms of action. In stable cavitation, the radial pulsations of MBs driven by the US field are controlled by the stiffness of the gas in the bubbles. Microstreaming around the bubbles could cause damage to nearby cells or fibers, or act to stir fresh fibrinolytic enzyme into otherwise inaccessible regions in a clot. In inertial cavitation, the radial motion of a bubble is controlled by the inertia of the rapidly moving liquid surrounding it. For symmetrical collapse, hot spots can form that can produce hydroxyl free radicals [25] capable of attacking nearby fibers. For asymmetrical collapse, microjets may form that can damage nearby fibers in the manner of pitting on ships' propellers. In all cases, US-driven bubbles might exteriorize new binding sites along fibers to allow fibrinolytic enzymes increased access.

MBs also had been applied to different kinds of application in recent years. Examples are gene or drug delivery, contrast agent in blood stream, and molecular imaging. MBs have been used in combination with ultrasound to improve the gene transfection and drug delivery efficiency. An in vitro study showed that, in inertial cavitation, the violent expansion, contraction and collapse of gas bubbles was related to hemolysis [26] and that the dose of inertial cavitation can be evaluated by measuring the power emitted during the cavitation process. Quantification methods for acoustic cavitation have been investigated by many researchers [26-29]. One method is to calculate the spectral broadband signal enhancement during MB destruction, since spectral spikes may appear at up to 30 to 40 MHz when MBs are destroyed [30]. Ultrasonic cavitation is thought to assist the delivery of molecules into a cell by transiently increasing the membrane permeability (also known as sonoporation) [31-36].
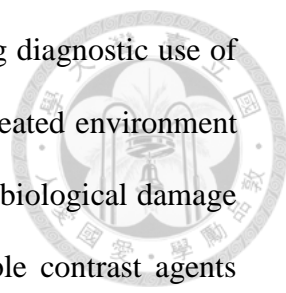
Thrombolytic therapy using enzymes plays an important role in cardiovascular disease, stroke, peripheral vessel diseases, and dialysis graft occlusion. However, there remain significant limitations of thrombolytic therapy, including speed of clot dissolution, resistance of some thrombi to fibrinolysis, and the occurrence of bleeding complications. Therapeutic use of ultrasound contrast agents is an emerging technique with potential in the areas of thrombolysis (clot dissolution), drug delivery and gene therapy [37]. The use of ultrasound in all these applications is desirable because it allows the non-invasive treatment of deep lesions (such as tumors and thrombi) with little or no effect on overlying tissues or organs. In the area of sonothrombolysis, a considerable amount of research has been directed towards the detection and treatment of blood clot (thrombus) associated with nonhemorrhagic stroke, myocardial infarction, deep vein thrombosis, and peripheral artery thrombosis [37-39]. It has been 30 years since thrombus dissolution with ultrasound was first reported [40]. However, the dissolution mechanisms still are not well understood. There are many influential factors for sonothrombolysis, including (but not limited to) clot morphology and age, physical and chemical environment, microbubble technology (if a contrast agent is involved), and therapeutic ultrasound dosage. Everbach and Francis (2000) demonstrated an increase in thrombolysis due to cavitation effects, but also suggested the possibility of other unknown mechanisms [41]. Cavitation is generally classified into two types, stable cavitation, which results in emissions at subharmonics of the main excitation frequency and inertial cavitation, which is characterized by broadband noise emissions [42]. Stable cavitation can induce bubble-associated micro-streaming and shear stress, while inertial cavitation can even cause micro-jetting and pitting on solid surfaces [42]. Datta and colleagues (2006) investigated stable and inertial cavitation as possible mechanisms for enhancing thrombolysis with a lytic drug t-PA. In
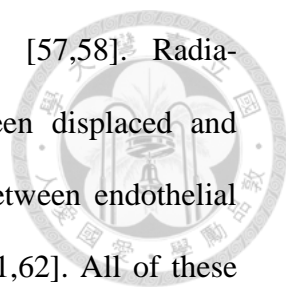
most of their experiments conducted above the stable cavitation but below the inertial cavitation threshold, cavitation was present almost throughout the entire exposure duration. In the ultrasound exposure condition above the inertial cavitation threshold, the inertial cavitation activity was sporadic and was often preceded or followed by stable cavitation activity. Therefore, sustaining stable cavitation for a longer period of time appears to be more effective in the thrombolysis enhancement than inertial cavitation [42]. Prokop and co-workers (2007) also studied the role of both inertial and stable cavitation during ultrasound-accelerated enzymatic fibrinolysis (with t-PA) in vitro in the presence and absence of Optison contrast MBs [43]. The addition of MBs significantly increased lysis. Inertial cavitation was present only at the start of the ultrasound exposure, while stable cavitation with low-amplitude subharmonic emissions persisted throughout. Their study indicated a potentially important role of stable rather than inertial cavitation in microbubble-enhanced sonothrombolysis. Even without the presence of any thrombolytic drug, the use of ultrasound contrast agents has been shown to increase the effectiveness of sonothrombolysis. Xie and colleagues (2005) investigated microbubble-mediated sonothrombolysis using a canine thrombus model that consists of a dialysis graft connecting femoral artery and vein [44]. In the graft occluded by thrombus, therapeutic ultrasound was applied during an intravenous infusion of MRX-815 MBs (ImaRx). Restoration of rapid flow (as an indicator of successful treatment) within the graft was seen.

This is particularly important in the form of inertial cavitation, which is the violent collapse of bubbles leading to very high localized increases in temperature and stress. Inertial cavitation generally requires a high ultrasound pressure (≥ 1.0 MPa) to activate the cavitation nuclei that are present in the medium. The nuclei may be submicroscopic gas bodies or MBs that are usually much smaller than bubbles that would

be resonant at biomedical ultrasound frequencies [8]. The emerging diagnostic use of ultrasound contrast agents may change a relatively poorly gas nucleated environment in the human body to a richly nucleated medium. Thus, the risk of biological damage may increase due to cavitation effects associated with microbubble contrast agents [45,46]. The concern regarding ultrasonic bioeffects has been raised by the observation of contrast-enhanced hemolysis and hemorrhage [28,47-52] both in vitro and in vivo. In vitro studies using human blood showed hemolysis at very high transmitted power levels [48]. Hemolysis in mice [49] and hemorrhage in the liver and kidney of anesthetized mice [50] were found using pulsed ultrasound at intensities utilized clinically, although at frequencies lower than those employed in medical imaging. Fortunately, no significant bioeffects have so far been found in animal models and humans (during clinical trials) from the use of US contrast agents such as Optison (Molecular Biosystems, Inc., San Diego, CA) at both intensities and frequencies of diagnostic US [51,53]. There is a paucity of studies on the mechanism of bioeffects associated with contrast MBs used in medical diagnostic US. This is partly owing to the complicated behavior of contrast MBs (when intensely insonified) resulting from their complex composition.

Applying low-intensity acoustic energy has been hypothesized as a way to move freely flowing contrast agents toward the endothelium [54,55]. Acoustic radiation forces (also known as Bjerknes forces) consist of two components: (1) a primary force directed away from the acoustic source in the direction of wave propagation and (2) a secondary attractive force that acts between individual bubbles. Dayton and colleagues verified that the primary radiation forces were able to displace nontargeted contrast agent away from the vessel center in a flow chamber [55,56] and in the mouse microcirculation [22]. The use of acoustic radiation forces has also been sug-

gested for enhancing the delivery of therapeutic substances [57,58]. Radiation-force-induced displacements may cause shear forces between displaced and non-displaced tissue, and the resulting strain may induce gaps between endothelial cells [59,60] and widen intercellular spaces in epithelial tissue [61,62]. All of these effects of radiation forces provide promise in targeting MBs onto a clot for sonothrombolysis. However, the characteristics of the shear forces induced by radiation forces are not yet fully understood in the thrombolysis model. Spengler et al. showed that radiation forces push the bubbles together in the fluid [63], while Sakharov et al. showed that acoustic streaming enhanced thrombolysis by an amount equivalent to that induced by mild stirring of a thrombolytic solution around the thrombus [64]. Nevertheless, the behavior of MBs inside mediums such as blood clots or tissues exposed to radiation forces is not fully understood.

Chemotherapy is one of the most important approaches for treating breast cancer patients. However, chemotherapeutic drugs such as PTX and doxorubicin lack cytotoxicity selectivity between cancer cells and normal cells, which frequently leads to serious side effects. Also, the poor water solubility of PTX makes it difficult to administer in clinical applications. Drug resistance and limited access of the drug often results in the drug concentration not been sufficiently high to kill malignant cancer cells [65, 66]. Therefore, localized drug delivery looks promising in reducing systemic toxicity and maximizing tumor exposure [67]. Drug-loaded-MBs destruction in combination with ultrasound has recently become one of the most promising therapeutic applications in drug delivery [68], since drug-loaded MBs can be manipulated and destroyed by ultrasound applied at the tumor site, causing localized release of the drug [69-72]. In addition, combining MBs with ultrasound can increase the permeability of physiologic barriers such as the blood–brain barrier, capillary endothelium,

and the cell membrane for macromolecules or even colloidal particles [73, 74]. Several investigations on the application of ultrasound contrast agents as tumor drug delivery systems have recently been reported. Kang et al. showed an antitumor effect of docetaxel-loaded lipid-shelled MBs combined with ultrasound-targeted MB activation on VX2 rabbit liver tumors [75]. Xing et al. demonstrated the effective treatment of ovarian carcinoma using PTX-loaded ultrasound MBs [76]. Tinkov et al. developed doxorubicin-loaded MBs with ideal physical characteristics and showed that their cytotoxic activity was enhanced relative to free doxorubicin and doxorubicin-loaded liposomes in in vitro experiments [77]. These studies have shown that shell-stabilized MBs can be used to load drugs or genes and improve the drug therapeutic index of a tumor when combined with ultrasound.

Chapter 2

Effects of Ultrasound-Induced Inertial Cavitation on Enzymatic Thrombolysis

2.1 Introduction

Ultrasound enhances enzymatic fibrinolysis both in vitro and in vivo [78–86]. Two approaches for sonothrombolysis are generally taken. The first approach delivers low-frequency (20–30 kHz) and high-intensity (>10 W/cm^2) ultrasound to the thrombus site via an intravascular transducer. Such an acoustic wave is capable of destroying thrombi and atherosclerotic plaques even without enzymatic thrombolysis. The most likely mechanisms of such destruction include vigorous cavitation (i.e., generation of active bubbles and cavities in the liquid), accompanying microstreaming, and direct mechanical fragmentation of the thrombus by vibration of the ultrasonic transducer tip [87,88]. Although several studies have demonstrated the efficacy of this approach both in animal models and patients using pulsed wave ultrasound [89–91], several problems remain, including potential perforation of vessel wall and embolization due to the release of large fragments of a thrombus [92,93], and local overheating. The other approach uses high-frequency (1–3 MHz) and low-intensity (0.5–5 W/cm^2) ultrasound. Such excitation can also be used for imaging and for destroying thrombi directly, but it can also enhance enzymatic fibrinolysis [79, 81, 82, 84, 86, 87, 94]. This approach is of particular interest because it can be applied noninvasively and transcutaneously. Nonetheless, the main concern of using high-frequency ultrasound is potential heating of the surrounding tissue, since heat production is proportional to

the ultrasound frequency.

Mechanisms underlying the enhancement of enzymatic fibrinolysis by ultrasound remain to be delineated, particularly because such enhancement could occur in clinical applications of ultrasound. Several mechanisms have been proposed for ultrasound in the kilohertz frequency range. Some studies have hypothesized that non-thermal mechanisms enhance the transport of fibrinolytic enzymes into the clot [95–97]. Suchkova et al. proposed that mechanical processes unrelated to cavitation could also be involved [98]. Sakharov et al. attributed the increase in lysis rate induced by 1 MHz ultrasound to an increase in enzymatic action due to a temperature increase, but concluded that this temperature rise constitutes a minor part of the enhancement effect of ultrasound [99]. They also concluded that ultrasound can produce acoustic streaming, which is effectively equivalent to mild stirring. Pieters et al. attributed the increase in thrombolysis when using 40-kHz ultrasound to an increase in penetration of the thrombolytic agent into the clot [100]. Their results were based on a clot model, and suggested the presence of multiple mechanisms resulting in the increased transport of thrombolytic agent into the clot. Nevertheless, the mechanism underlying the transportation of the thrombolytic agent into the clot remains unclear.

Enzymatic thrombolysis might also be attributable to cavitation effects. Cavitation is generally classified into two types: stable and inertial. Stable cavitation results in the emission of subharmonics of the main excitation frequency and induces bubble-associated microstreaming [24], whereas inertial cavitation emits broadband noise and induces microjetting and pitting on solid surfaces [101, 102]. Everbach and Francis demonstrated that cavitation increases thrombolysis, but they were unable to distinguish between stable and inertial cavitation [41]. Some investigators have clearly shown that ultrasound accelerates enzymatic fibrinolysis by increasing the transport of

reactants via cavitation-related mechanisms [79,82,103]. Koch et al. provided evidence that ultrasound-assisted drug uptake is due to cavitation [103]. The results of these previous studies indicate that the respective roles of stable and inertial cavitation need to be further examined.

The optimal condition of ultrasound-assisted enzymatic thrombolysis still needs to be determined. High-frequency ultrasound is more promising for avoiding embolization and perforation of vessel wall during sonothrombolysis due to the ability to focus at depth. Our previous study of the use of sonoporation to deliver DNA into cells suggested that inertial cavitation plays a role in thrombolysis [104]. Thus, the main purpose of the present study was to elucidate the effects of individual acoustic parameters (amplitude and duration) as well as the microbubble concentration on the reduction in the weight of a blood clot. The combined effects when also using thrombolytic enzyme were also evaluated. This study was also motivated by the possibility of using the measured cavitation effects for sonothrombolysis to take the place of weight measurement in vivo.

2.2 Materials and Methods

2.2.1 Blood Clot Preparation and Examination

After obtaining our ethics committee's approval and informed consent from volunteer, fresh human blood was drawn and divided into 0.2-ml Eppendorf tubes (Scientific Specialties, Lodi, CA, USA). Each tube contained 100 μl of blood and 10 μl of 0.5 M calcium chloride (Sigma-Aldrich, St. Louis, MO, USA). All samples were kept at 25°C for 24 hours to ensure complete solidification and consistency of the blood clots. The blood clots were weighed before and after each ultrasound treatment to de-

termine the induced weight reduction. Before weighing, the clot was removed from the Eppendorf tube and placed on a paper towel to remove the superfluous liquid.

After experiments, the blood clots were fixed with formaldehyde, embedded with paraffin, sliced, and stained for microscopy examinations (CKX41, Olympus, Japan) and photography. The blood clots of the same group were placed on a single slide.

2.2.2 Preparation of MBs

We used two types of MBs in our experiments: (1) phospholipid-shelled MBs (SonoVue, Bracco, Amsterdam, Netherlands) and (2) albumin MBs made using our in-house protocols [106]. The concentration of the SonoVue MBs was about $1–5×10^8$ /ml (5 mg/ml).

After mixing human albumin (Octapharma, Lachen, Switzerland) with normal saline into a 3% solution, it was ventilated with perfluoropropane and sonicated for 2 min, then incubated on ice for 5 min. The concentration of the MBs was more than $8×10^9$ /ml, their diameters were 1.0–4.0 μm with a mean of 1.9 μm (Multisizer 3, Beckman Coulter, Fullerton, CA, USA), and their half-life was more than 3 hours. The MBs were diluted to the desired concentration just before experiments.

2.2.3 Ultrasound Thrombolysis System

The setup for acoustic measurements (Fig. 2) allowed measurements of the inertial cavitation dose (ICD), which was proved as an effective tool for detecting and analyzing inertial cavitation [105].
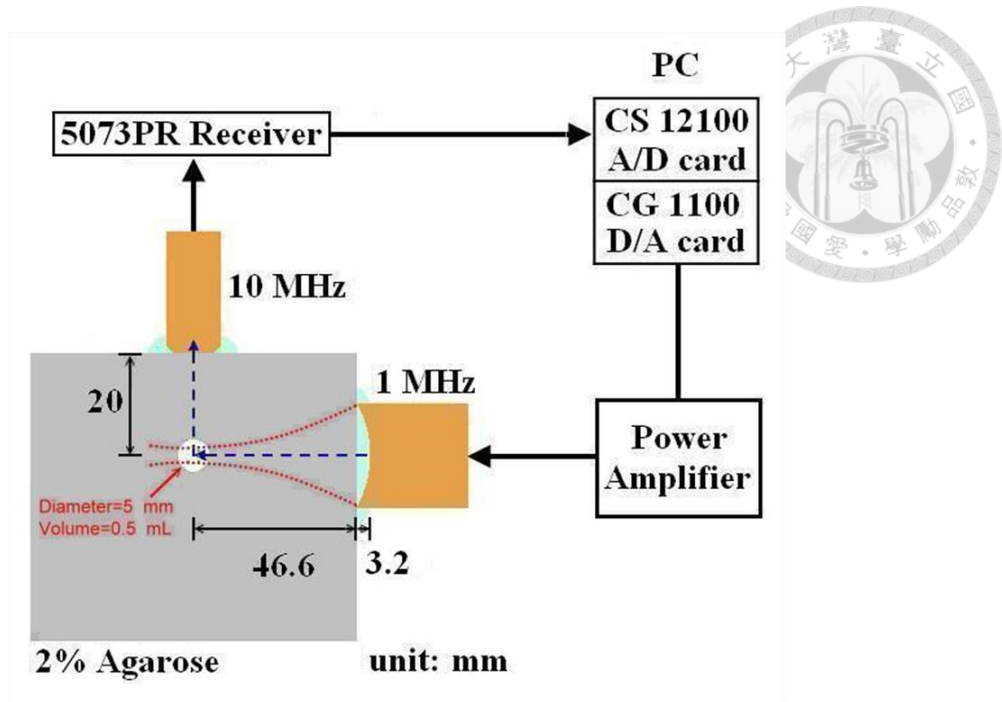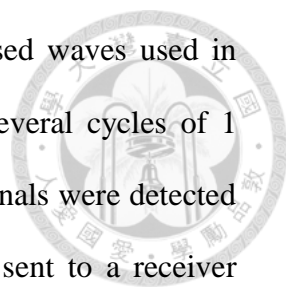
Fig. 2. Setup for acoustic cavitation measurements.

A 10 MHz transducer was used to detect the broadband signal enhancement and to avoid harmonics of the 1 MHz transmitted signals. The incident amplitude of the harmonic at 10 MHz and the received subharmonic signal at 0.5 MHz were minimal. The received signal was then quantified as the root-mean-square (RMS) value in the time domain between 9.5 and 10.5 MHz and integration over time. Finally, the background time-amplitude curve (the measured RMS amplitude from water only) was subtracted and the resulting amplitude is referred to as the differential ICD that was used for subsequent signal analysis. In our model system, a 1.0 MHz focused transducer (V302, Panametrics-NDT, Waltham, MA, USA) with a diameter of 25.4 mm and a focal length of 49.8 mm was used for transmission. The beam width and depth of field of the transducer were 6.0 mm and 55.0 mm, respectively. The transmitted waveforms were generated by a digital-to-analog converter (CompuGen 1100, GaGe Applied Technologies, Lachine, QC, Canada) and amplified by a power amplifier

(250A250A, Amplifier Research, Souderton, PA, USA). The pulsed waves used in this study had a repetition frequency of 100-Hz, which means several cycles of 1 MHz waves followed by a rest of 10 milliseconds. The acoustic signals were detected by an unfocused 10 MHz transducer (V312, Panametrics-NDT), sent to a receiver (5073PR, Panametrics-NDT), digitalized by an analog-to-digital converter (CompuScope 12100, GaGe Applied Technologies), and analyzed using MATLAB (MathWorks, Natick, MA, USA). A 2% agarose phantom was made with a cylindrical cavity (5 mm in diameter and 25 mm deep) to contain the blood clot. The 1 MHz transducer was positioned with the －6-dB focal zone covered the entire cavity, as shown in figure 2, while the unfocused 10 MHz transducer with a diameter of 6.4 mm was placed at 20 mm from the cavity. The overall ultrasound exposure duration was 1.5 second.

2.2.4 Experimental Design

We first evaluated the individual effects of the acoustic amplitude (by varying the driving voltage to the transducer), pulse duration (by varying the number of cycles of the transmit waveform), and microbubble concentration (by SonoVue) on thrombolysis. Each measurement in different concentrations, cycle numbers and voltage settings were repeated five times to reduce human and system errors. The effects of MBs on thrombolysis were investigated at concentrations of 0 (as control), 0.25, and 0.5 mg/ml with a fixed driving voltage of 5 volts and a pulse duration of 10 cycles. The effects of driving voltages of 0 (as control), 1, 2, and 5 volts were compared with a fixed microbubble concentration of 0.5 mg/ml and a pulse duration of 10 cycles. The acoustic pressures produced with driving voltages of 1, 2, 5 volts were 0.52, 0.94, 1.30 MPa, respectively. Finally, pulse durations of 1 (as control), 2, 5, and 10 cycles were examined with a fixed driving voltage of 5 volts and a microbubble concentra-

tion of 0.5 mg/ml. The duty cycle for 10 cycle pulses, for example, equals to 0.1%. We then compared the respective effects of ultrasound, MBs (albumin-shelled, in house), and streptokinase on thrombolysis relative to the results for the above experiments. The blood clot without being exposed to any of these effects was used as control. On the other hand, the experimental groups include ultrasound, ultrasound with MBs, streptokinase, and ultrasound with MBs after streptokinase exposure. The measurements were repeated eight times in control and each experimental groups to reduce human and system errors. Streptokinase (Sigma-Aldrich, St. Louis, MO, USA) was introduced into the Eppendorf contained blood clot to produce a final concentration of 1000 U/ml for 30 min at 25°C. Then the blood clot was taken out and placed into phantom cavity for subsequent ultrasound and microbubble applications. The differential ICD (dICD) was calculated as the difference in ICD between the experimental and control groups. The ICD values of all control groups were checked and found equal to the ICD value of water.

2.2.5 Statistics

The obtained results are given here as mean and standard deviation values and compared using the Wilcoxon-Mann-Whitney test. A probability value of $P < 0.05$ was considered statistically significant.

2.3 Results

Figure 3 shows the relationships between clot weight reduction and dICD for different pulse durations, driving voltages, and microbubble concentrations. The weight reduction percentages and ICD values of all the control groups were set as ze-

ro in figure 3. Figure 3a shows that the weight reduction of a blood clot and the cavitation effect as evaluated by dICD increased approximately monotonically with the driving voltage. Lower voltages produced negligible effects since inertial cavitation did not occur. Figure 3b shows that the weight reduction of a blood clot and the dICD increased with the pulse duration. Figure 3c shows that the weight reduction of a blood clot and dICD increased monotonically with the microbubble concentration. Higher concentrations were tested and found that the thrombolysis effects were reduced. This can be explained by the increased shielding effect of MBs. A scatter plot with the linear regression of clot weight reduction versus dICD from the data in figures 3a to 3c is shown in figure 3d, for which the correlation coefficient was 0.66.
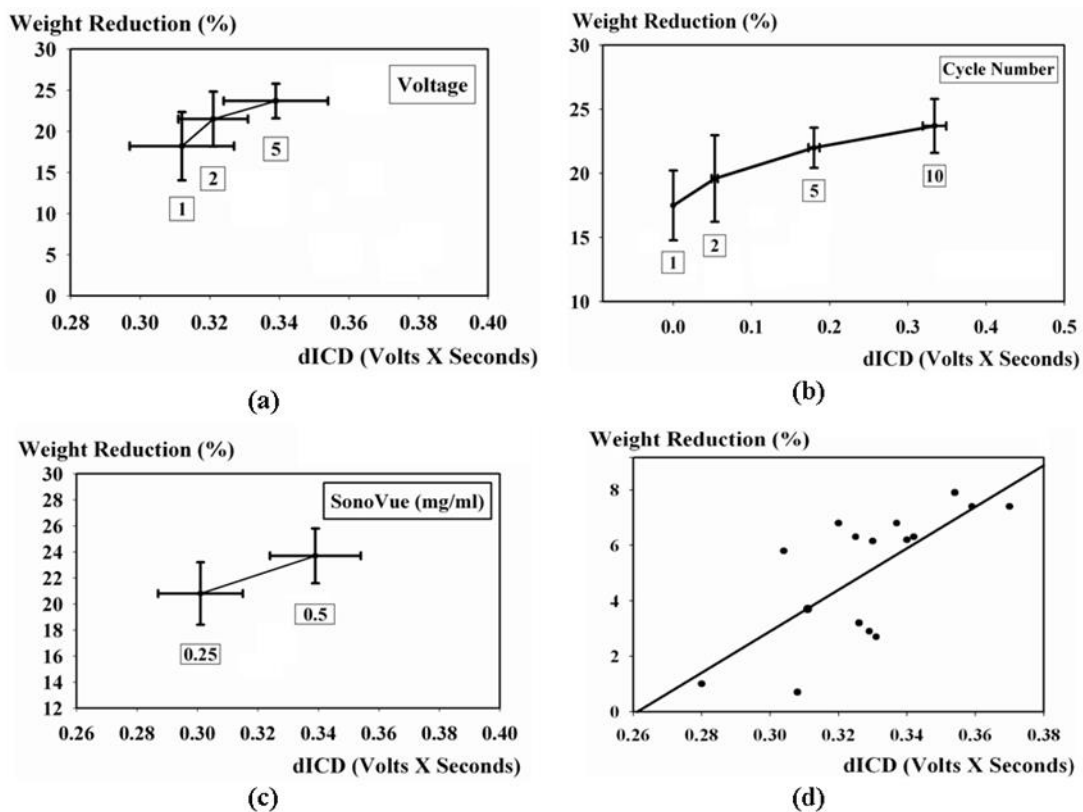

Fig. 3. Relationships between dICD and clot weight reduction for different cavitation parameters: (a) driving voltage, (b) pulse duration, and (c) microbubble concentration. (d) Linear regression of the experimental data.
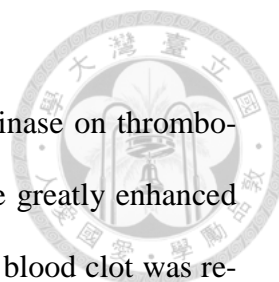
Figure 4a shows the effects of ultrasound, MBs, and streptokinase on thrombo-lysis. The figure shows that the effects of sonothrombolysis can be greatly enhanced by combining ultrasound, MBs, and streptokinase. The weight of a blood clot was reduced by about 50% in experiments. In contrast, the ICD values in sonothrombolysis, and shows that adding streptokinase to microbubble-induced inertial cavitation had no significant effect ($P<0.01$) on the ICD value (Fig. 4b). By comparing figures 3a, 3b, and 4a, we found that these two types of MBs exerted similar effects on sonothrom-bolysis (by weight reduction and ICD evaluation) for the experimental parameters we used.
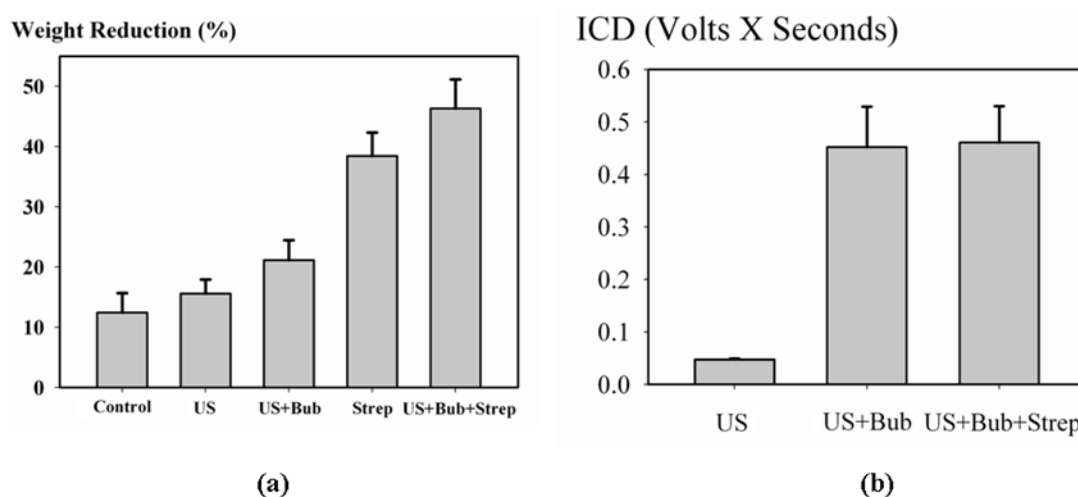

Fig. 4. Individual effects of ultrasound, MBs, and streptokinase on thrombolysis as evaluated by clot weight reduction (a) and ICD (b). Data are mean and standard deviation values.

Figures 5 and 6 are microscopy images of blood clots at two magnifications, and show that the blood clot of the control group (Fig. 5a) had an intact smooth surface, with higher magnification (Fig. 6a) revealing an intact red blood cell and clot struc-ture. Since whole blood was used in the experiment, the blood clot consisted of hya-line and red parts (mainly red blood cells). Blood clot exposed to ultrasound alone

(Figures 5b and 6b) show intact red blood cells that have separated from the surface or loosened within a certain depth of the blood clot on the exposure side. Exposure to ultrasound and MBs (Fig. 5c) produced a rough and porous surface (about 25 μm in depth) on the blood clot. Damaged red blood cells were evident around the surface (Fig. 6c, arrowhead). Blood clots exposed to streptokinase showed significant shrinkage in global size and disappearance of fibrin clots (the hyaline part) in observation. Figures 5d and 6d showed the irregular surface of the clot created by Streptokinase, while remaining the red blood cells intact. Figure 5e shows a clot exposed to ultrasound, MBs, and thrombolytic enzyme simultaneously. Several large cavities with average depth of about 200 μm can be seen within the clot and distributed on the exposed side in every clot slice. Some cavities were close to the surface (indicated by arrowheads in the figure), while others were deep inside the clot. The side of the clot opposite to the side of ultrasound exposure looked the same as that in the streptokinase group (Fig. 5d), without the presence of cavities. Also, damaged red blood cells were readily identifiable in this experimental group (Fig. 6e, arrowheads). Comparing Figures 5e and d, it is possible that streptokinase not only induced lysis on the surface, but also penetrated into the blood clot and subsequently helped to enlarge the cavities.
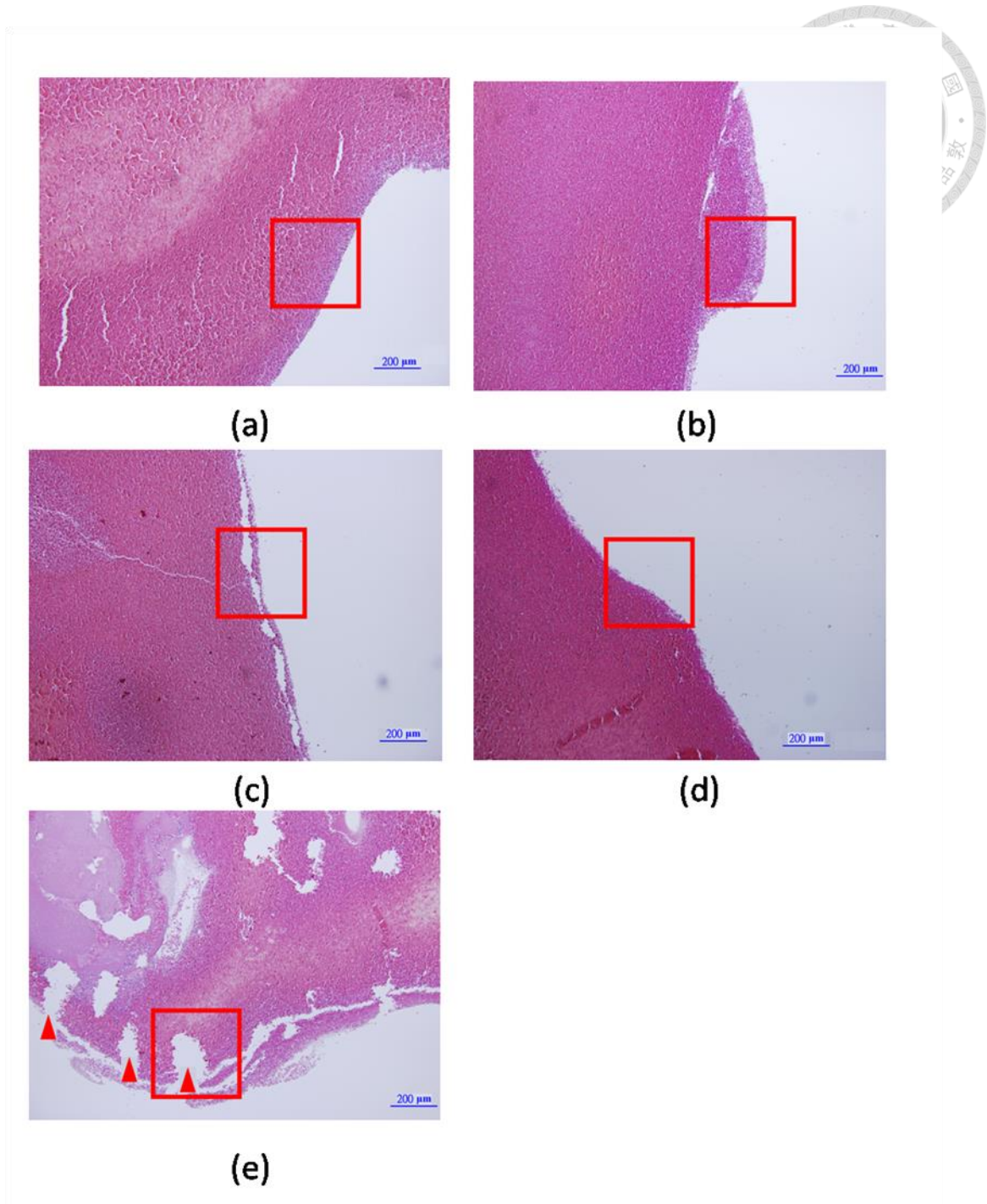
Fig. 5. Microscopy images of blood clots for control (a), ultrasound (b), combined ultrasound and MBs (c), streptokinase (d), and combined ultrasound, MBs, and streptokinase (e). Arrowheads indicate the inlets of cavities. Rectangles indicate the area magnified in Fig. 6.
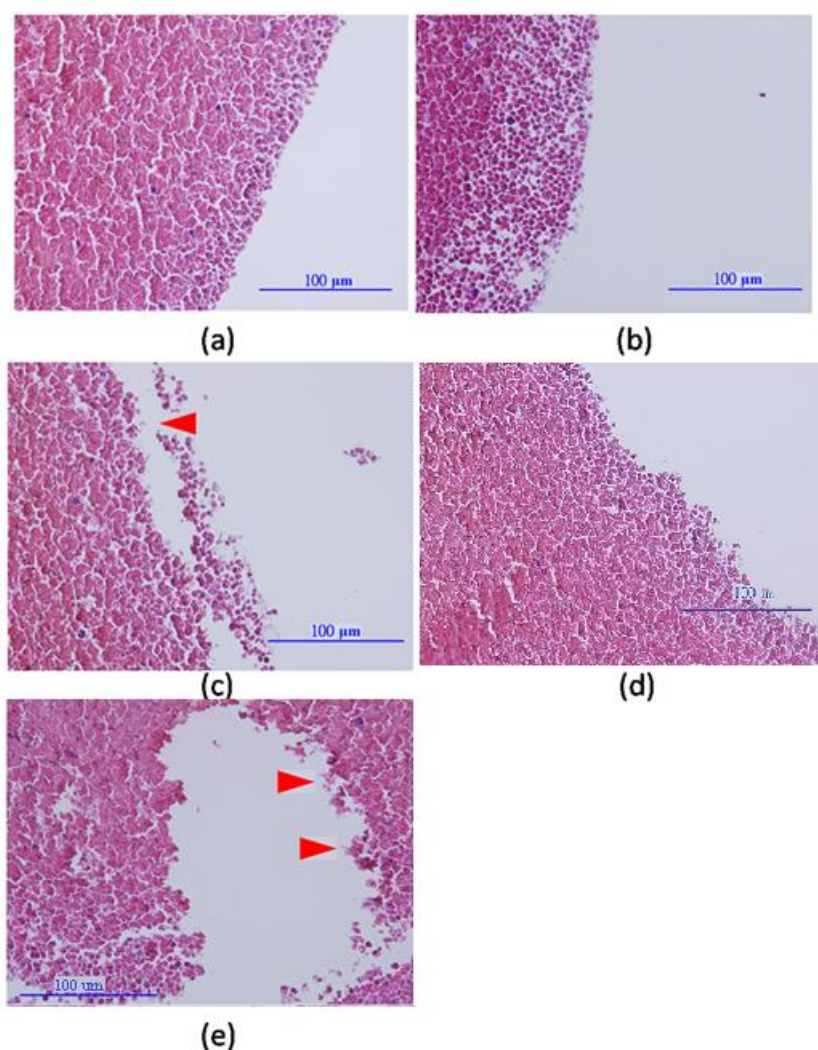
Fig. 6. Microscopy images of blood clots (at higher magnification) for control (a), ultrasound (b), combined ultrasound and MBs (c), streptokinase (d), and combined ultrasound, MBs, and streptokinase (e). Arrowheads indicate damaged red blood cells.

2.4 Discussion

Combining ultrasound, MBs, and thrombolytic agent appears to be a promising method for sonothrombolysis. Cavitation (especially inertial cavitation) probably underlies ultrasound-enhanced thrombolysis. The ICD we previously proposed was

proved to be a useful indicator of thrombolysis in this study [81]. In addition to the present investigation of inertial cavitation, future studies of stable cavitation would help further the understanding of the mechanisms underlying enzymatic sonothrombolysis.

Sakharov et al. attributed the increase in lysis rate induced by 1-MHz ultrasound to an increase in enzymatic action due to a 6°C temperature rise, but concluded that this temperature rise constituted a minor part of the enhancing effect of ultrasound [64]. Our experimental results are consistent with this conclusion. Ultrasound was applied in our experiments for 1.5 seconds after the blood clot had been soaked in streptokinase for 30 min. The temperature might increase, but the ultrasound duration is too short for this factor alone to produce the significant changes shown in figure 5e (relative to figure 5d). Sakharov et al. also concluded that the effect of ultrasound is equivalent to mild stirring, possibly caused by acoustic streaming. Our results indicate that inertial cavitation played a major role in producing cavities (Fig. 5e, arrowheads), with microjetting creating pitting on the surface, subsequent carving by MBs, and their size being increased by enzymes. Another notable feature was the damage to red blood cells. Since MBs and red blood cells are similar in size (1–2 versus 7 μm, on average), inertial cavitation can also happen on the surface of blood cells. The presence of fragments of red blood cells in figure 6e supports this hypothesis. Applying acoustic cavitation alone without enzyme, as in figure 5c, also elicited microjetting on red blood cells. Further evidence of inertial cavitation was microbubble debris coming up to the solution surface within about 5 seconds after ultrasound exposure, with the solution becoming clear at the same time; without ultrasound irradiation, the solution remained cloudy. This indicates that MBs ruptured soon after being exposed to ultrasound and produced inertial cavitation, as demonstrated by Prokop et al. The residual

microbubble concentration was believed to be too low for stable cavitation to play a major role in our experiments [43].

The microscopic differences between streptokinase alone (Fig. 5d) and combined ultrasound, MBs, and streptokinase (Fig. 5e) indicate that the enzyme already infiltrated into the clot during the 30 min of deposition. The thrombolytic enzyme streptokinase digested the fibrin clot macroscopically and possibly loosened connections among red blood cells within the clot by diffusion. The further application of ultrasound and MBs readily enlarged the cavities (compared to figure 5c and 5e) by inertial cavitation. The role of enzyme is relatively limited during the 1.5 second exposure of cavitation. Francis et al. suggested the mechanical forces associated with ultrasonic radiation might push MBs and enzyme to penetrate the surface layer of red blood cells in their study [103]. The relatively short duration of ultrasonic radiation in our study makes the penetration of MBs and enzyme less significant. From these observations we can conclude that transport of fibrinolytic enzyme into clots significantly affects the rate of fibrinolysis.

Stable cavitation has been shown to play an important role in sonothrombolysis [42,64]. The acoustic pressure used in the present study (1.30 MPa) falls within the range that induces inertial cavitation. Stable cavitation was expected to exert relatively insignificant effects in our model. These observations suggest that the type of cavitation and its relative contributions on thrombolysis vary with the acoustic pressure and model system. However, our study further indicates the importance of cavitation effects in enzymatic thrombolysis. Future studies should investigate the mechanisms of cavitation in thrombolysis, particularly stable cavitation.

2.5 Conclusions

This study has demonstrated the effects of acoustic inertial cavitation in sonothrombolysis. The transportation of fibrinolytic enzyme into clots significantly affects the rate of fibrinolysis. Moreover, the ICD is potentially a useful tool for sonothrombolysis evaluation, since weight reduction measurement of thrombus is not applicable clinically. Nonetheless, the relative contributions in enzymatic thrombolysis by different types of cavitation were still undetermined and require further studies for better understanding.
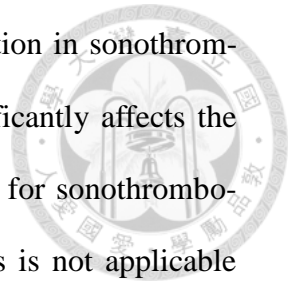
Chapter 3

Combining Radiation Forces with Cavitation for Enhanced Sonothrombolysis

3.1 Introduction

The presence of thrombi or emboli within blood vessels can lead to various clinical diseases, including myocardial infarction, peripheral artery disease, deep vein thrombosis, and acute ischemic stroke. Such diseases remain the leading causes of death in many developed countries. Ultrasound has been used for several decades to promote clot breakdown as both a stand-alone treatment and in combination with thrombolytic agents, and more recently in combination with ultrasound contrast agents, both in vitro and in vivo [79,86,107-115]. However, the specific mechanisms have yet to be elucidated, and its safety and efficacy remain to be optimized.

Cavitation is one of the possible mechanisms underlying sonothrombolysis. Recent data suggest that stable cavitation is more effective than inertial cavitation for clot lysis [42]. The disadvantages of cavitation-induced sonothrombolysis include damage to the endothelium, perforation of the vessel wall, and platelet activation. It is possible that such problems can be alleviated by making the exposure area smaller using targeted MBs or the "push effect" provided by acoustic radiation forces. In molecular imaging studies, MBs are tagged with an adhesion ligand that binds to molecular markers expressed on a diseased endothelium, which retains the contrast agent preferentially at sites exhibiting characteristics such as inflammation, angiogenesis, or thrombus [116–120]. However, the microvascular rheology of several nontargeted

microbubble preparations has been shown to be very similar to that of erythrocytes [121–123], and microscopy observations have confirmed that MBs tend to distribute toward the axis of the vessel [124], with only few exceptions [125–127]. Thus, the frequent absence of contrast agent contacting the target surface may be a significant impediment to applications.

Applying low-intensity acoustic energy has been hypothesized as a way to move flowing contrast agents toward the endothelium and named radiation force [54,55]. Acoustic radiation forces (also known as Bjerknes forces) consist of two components: (1) a primary force directed away from the acoustic source in the direction of wave propagation and (2) a secondary attractive force that acts between individual bubbles. Dayton and colleagues verified that the primary radiation forces were able to displace nontargeted contrast agent away from the vessel center in a flow chamber [55,56] and in the mouse microcirculation [22]. The use of acoustic radiation forces has also been suggested for enhancing the delivery of therapeutic substances [57,58]. Radiation-force-induced displacements may cause shear forces between displaced and non-displaced tissue, and the resulting strain may induce gaps between endothelial cells [59,60] and widen intercellular spaces in epithelial tissue [61,62]. All of these effects of radiation forces provide promise in targeting MBs onto a clot for sono-thrombolysis. However, the characteristics of the shear forces induced by radiation forces are not yet fully understood in the thrombolysis model. Spengler et al. showed that radiation forces push the bubbles together in the fluid [63], while Sakharov et al. showed that acoustic streaming enhanced thrombolysis by an amount equivalent to that induced by mild stirring of a thrombolytic solution around the thrombus [64]. Nevertheless, the behavior of MBs inside mediums such as blood clots or tissues exposed to radiation forces is not fully understood.

In this study we examined the ability of acoustic radiation forces to enhance the active targeting of MBs in a cavitation-induced sonothrombolysis model with a flow phantom system. The interaction between MBs and the clot was examined by confocal microscopy.
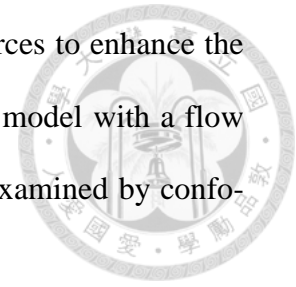
3.2 Materials and Methods

3.2.1 Blood Clot Preparation and Examination

The samples in experiments come from a volunteer after documentation of informed consent and institution review board. Freshly drawn human blood was mixed with biotin-NHS (Cayman Chemical, Ann Arbor, MI, USA) (final concentration 0.08%), and 100-µl aliquots added to 200-µl PCR tubes (Scientific Specialties, Lodi, CA, USA). Biotin-NHS binds to proteins on red blood cells (RBC), and makes it possible to trace avidin-albumin MBs in the blood clot after experiments. All samples were kept at 37°C in a water bath for 24 hours to ensure that consistent clots were formed. The blood clots were weighed before and after each ultrasound treatment to determine their weight loss.

After ultrasound exposure, the blood clots were fixed with 10% formaldehyde, embedded with paraffin, sliced, fixed on slides, and stained with 0.01% biotin-4-FITC (AnaSpec, San Jose, CA, USA) for confocal microscopy examination (TCS SP2, Leica, Heidelberg, Germany) and photography. Biotin-4-FITC, which binds avidin specifically, was used to visualize the distribution of avidin-albumin MBs after ultrasound exposure. The photographs from confocal microscope were converted into 8-bit gray-scale images. In each image, we chose 10 lines that were perpendicular to the clots surface for fluorescence study. For each line we calculated the average fluores-

cence intensity per unit distance. Then, the intensity and depth data from those lines in each image were averaged for demonstration and further analysis.

3.2.2 Microbubble Preparation

After mixing the human albumin (Octapharma, Lachen, Switzerland) and avidin (ThermoScientific, Rockford, IL, USA) with normal saline at 3% and 0.04%, respectively, the solution was ventilated with perfluoropropane and sonicated (S-450D, Branson Ultrasonic Corp, Danbury, CT, USA) in 280 Watt for 2 min, and then incubated on ice for 30 min. The concentration of the MBs was more than 8×10^9/ml, and they had a mean diameter of 1.9 μm (range 1.0–4.0 μm) (Multisizer 3, Beckman Coulter, Fullerton, CA, USA), which changed less than 1% over 3 hours at 4°C. The MBs were diluted with normal saline to the desired concentration prior to experiments.

3.2.3 Flow Cytometry Examination

In order to confirm that avidin integrates into the albumin shell and remains active after forming avidin-albumin MBs, we added biotin-4-fluorescein (AnaSpec, final concentration 0.01%) into the avidin-albumin microbubble solution (final concentration 0.04% and 1.2%, respectively), incubated at room temperature for 15 min with light protection, washed it with normal saline by centrifugation (1500 rpm for 5 min) for three times, and then used flow cytometry to measure the fluorescence of the MBs. The avidin that remained active on MBs would bind biotin molecules, and this was counted by flow cytometry. Also, we used streptavidin-FITC (AnaSpec) to determine whether sufficient biotin-NHS molecules binds to red blood cells and remains active. Freshly drawn human blood was washed with normal saline and centrifuged (1500

rpm for 5 min) to remove serum protein. Biotin-NHS was added with final concentration of 0.08%, incubated at room temperature for 1 hour, washed three times by centrifugation. The streptavidin-FITC (final concentration 0.04%) was then added, incubated at room temperature for 15 min with light protection, washed by centrifugation, and counted by flow cytometry.

3.2.4 Ultrasound System

The acoustic measurement setup is shown in Fig. 7. A 1.0-MHz transducer (V302, Panametrics-NDT, Waltham, MA, USA) with a diameter of 25.4 mm and a focal length of 49.8 mm. was used for transmission. The transmitted waveforms were generated by a digital-to-analog converter (DA card) (CompuGen 1100, GaGe Applied Technologies, Lachine, QC, Canada) and amplified by a power amplifier (250A250A, Amplifier Research, Souderton, PA, USA). The acoustic signals were detected by an unfocused 10-MHz transducer (V312, Panametrics-NDT) and sent to a receiver (5072PR, Panametrics-NDT). Pulsed waves were used in this study with a repetition frequency of 100 Hz, pulse duration of 10 cycles, exposure time of 1.5 sec, and acoustic pressures of about 1.32 MPa for cavitation settings [115]. A 2% agarose phantom was constructed with a cylindrical cavity (5 mm in diameter and 2.5 cm deep) to hold the blood clot and a tilting tunnel (2.7 mm in diameter) passing through the cavity. A continuous flow (5 ml/min) of MBs solution was provided by a syringe pump (KD Scientific, Holliston, MA, USA) to simulate the human arterial blood flow [128]. The microbubble solution comes out from the orifice of the flow phantom (shown by the arrow on the left of the 10-MHz transducer). It is lower than the orifice of sample cavity to make sure the flow rate is consistent within the system. Both transducers were positioned with their focuses within the cavity. Temperature remains

at 25℃ during experiments. Further analysis and calculation of the inertial cavitation dose (ICD) were performed using MATLAB (Mathworks, Natick, MA, USA) [105].
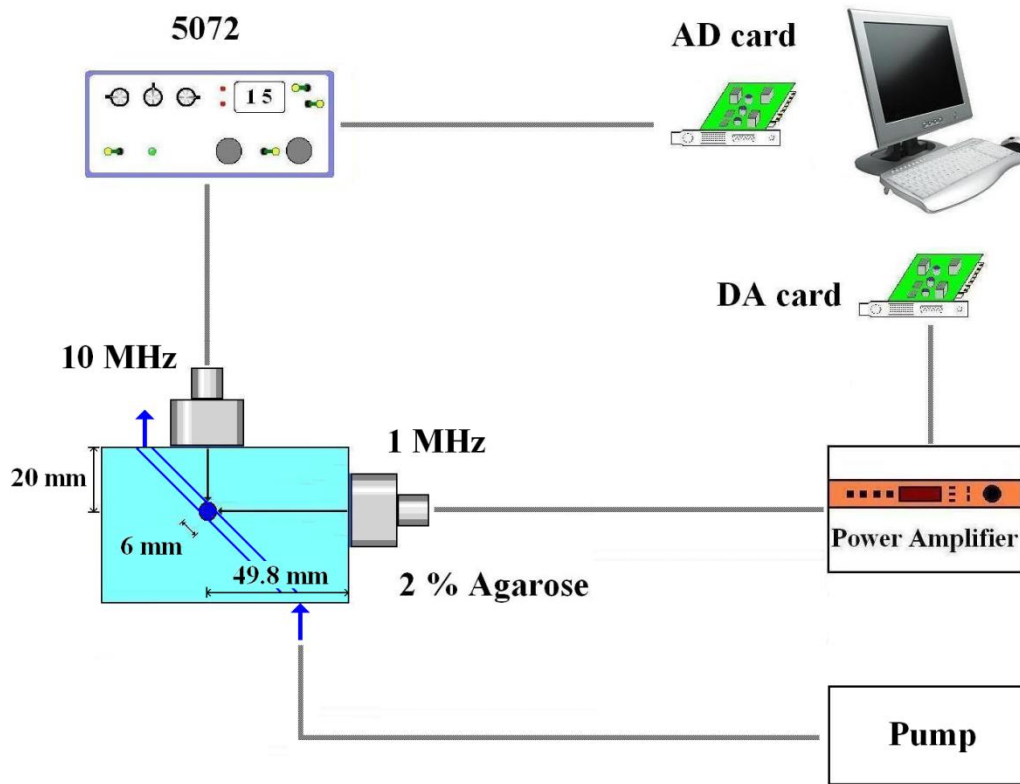

Fig. 7. Experimental setup.

3.2.5 Radiation Force Setting

Before experiments, we used the phantom model mentioned above to find out the radiation-force acoustic settings. A 6.7 MHz probe (10L, GE, Tokyo, Japan) of an ultrasound machine (LOGIQ 500, GE, Tokyo, Japan) was placed opposite to the 10 MHz transducer to evaluate the movement of MBs. Radiation force produced by 1 MHz transducer was imaged by the GE system as the MBs pushed away from the transducer. Minimal cavitation effect presented in ICD was recorded. The radiation force settings included a pulse wave with a repetition frequency of 100 Hz, pulse du-

ration of 100 cycles, exposure time of 1.5 sec, and acoustic pressures of about 0.12 MPa.

3.2.6 Experimental Design

The experiments were divided into four groups [control, radiation forces, cavitation, radiation forces combined with cavitation (RF+Cav)], with the ten data samples collected within each group averaged to reduce human and system errors. The RF+Cav group was exposed to acoustic radiation forces followed by cavitation settings, and repeated these two acoustic exposures for 10 times (in order to maximize the effect). The radiation-force group and the cavitation group were also exposed 10 times to their respective stimuli to allow accurate comparisons. Different microbubble concentrations were used in the experiments. The samples in the control group without ultrasound exposure were immersed in a solution containing MBs at a concentration of 4×10^7/ml.

3.2.7 Statistics

Kruskal-Wallis one-way ANOVA was used to statistically compare between the experimental groups, with a *P* value of less than 0.05 considered to be indicative of significance.

3.3 Results

Fig. 8 shows the flow cytometry results of avidin on albumin MBs and the binding condition of biotin-NHS on red blood cells. The black line (solid arrow) in Fig. 8(a) indicates that no biotin-4-fluorescein could bind albumin MBs without avi-

din, while the gray line indicates fluorescence on MBs. This figure indicates that avidin did integrate into the albumin shell of the MBs and remains active. The gray line on the right side of Fig. 8(b) indicates that biotin-NHS was detected on red blood cells, while the gray line on the left side of the figure (hollow arrow) indicates the fluorescence staining of red blood cells without biotin-NHS binding. The black line (solid arrow) indicates the background fluorescence of the cells. This figure indicates that biotin-NHS binds to red blood cells and remains active.
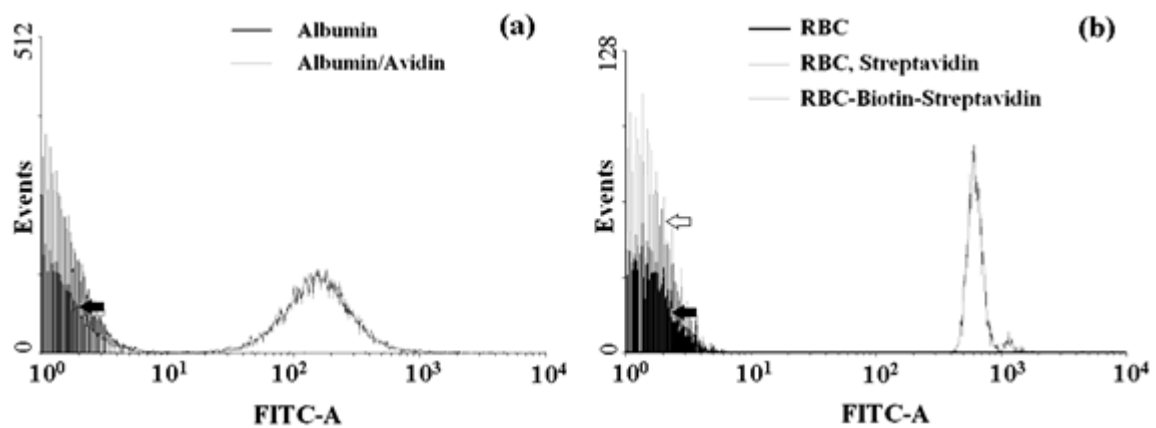

Fig. 8. Flow cytometry results. (a) Avidin and albumin MBs. (b) Biotin-NHS and red blood cells (RBC).

Fig. 9(a) shows the effects of radiation forces, cavitation, and radiation forces combined with cavitation on blood clots for different microbubble concentrations based on measurements of the weight reduction. Fig 9(b) indicates the cavitation intensity during the same set of experiments. The weight reduction produced by cavitation increased with the bubble concentration [Fig. 9(a)], as did the cavitation effect as evaluated by the ICD [Fig. 9(b)], relative to the control group. The ICD of control group represents the background level of cavitation for comparison. Both results are

statistically significant (p<005). The radiation forces alone exerted minimal effects on the weight reduction of the blood clot and ICD, relative to the control group, even if the bubble concentration increases. The statistics are insignificant. However, the RF+Cav group showed additional 3–9% weight reductions of thrombi relative to the cavitation group as the microbubble concentration increased and statistically significant (p<005). The ICD differences between the RF+Cav and cavitation group in the same bubble concentration are statistically insignificant. The discrepancy in weight reduction and ICD results between RF+Cav and cavitation groups is explained by the radiation force applied before cavitation effect in RF+Cav group.
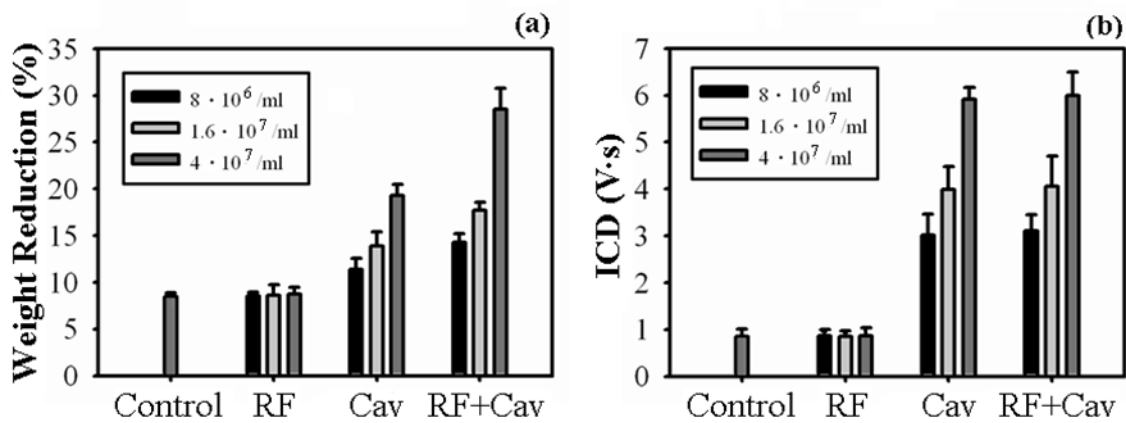

Fig. 9. Effects of radiation forces (RF), cavitation, and radiation forces combined with cavitation (RF+Cav) on thrombolysis for different microbubble concentrations. (a) Weight measurement. (b) ICD evaluation.

Figs. 10–12 demonstrate the fluorescence distribution and intensity of blood clots after ultrasound exposure. The fluorescence on the clot presents the distribution of avidin-albumin MBs, but it does not record the total acoustic effects ever exposed in individual experimental group (including sonothrombolysis). The distribution of MBs on the clot is described by the fluorescence intensity and depth from the clot

surface. Comparing all of the radiation-force groups in Figs. 10–12 reveals that the fluorescence intensity on the clot increased with the microbubble concentration. Similar results can be seen for the cavitation-alone and radiation force combined with cavitation groups. We also observed that the distance that MBs traveled from the clot surface varied with the acoustic exposure and microbubble concentration. Here we hypothesize that radiation forces combined with cavitation enhanced microbubble distribution into the clot.
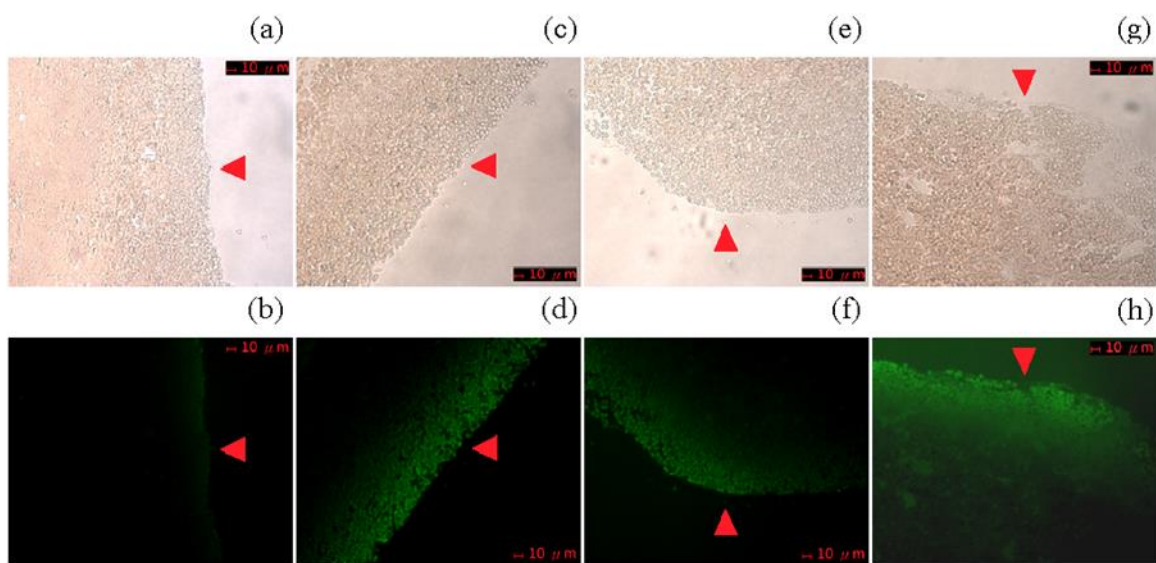

Fig. 10. Confocal microscopy photographs of blood clots. Upper and lower rows are in color and FITC fluorescence mode, respectively. Microbubble concentration is 4×10^7/ml. Red arrowheads indicate the clot surface. (a) and (b) are control group. (c) and (d) are radiation force group. (e) and (f) are cavitation group. (g) and (h) are radiation force combined with cavitation group. The photographs in the same experimental group are from the same slice.
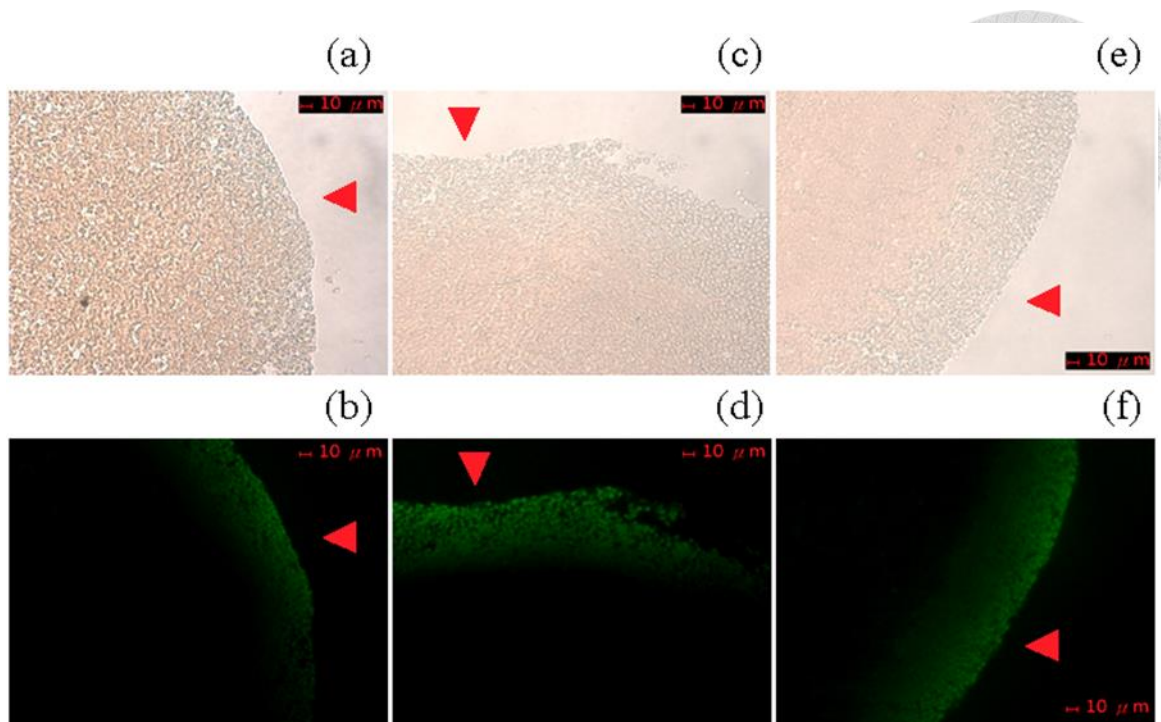
Fig. 11. Confocal microscopy photographs of blood clots. Upper and lower rows are in color and FITC fluorescence mode, respectively. Microbubble concentration is 1.6×10^7/ml. Red arrowheads indicate the clot surface. (a) and (b) are radiation force group. (c) and (d) are cavitation group. (e) and (f) are radiation force combined with cavitation group. The photographs in the same experimental group are from the same slice.
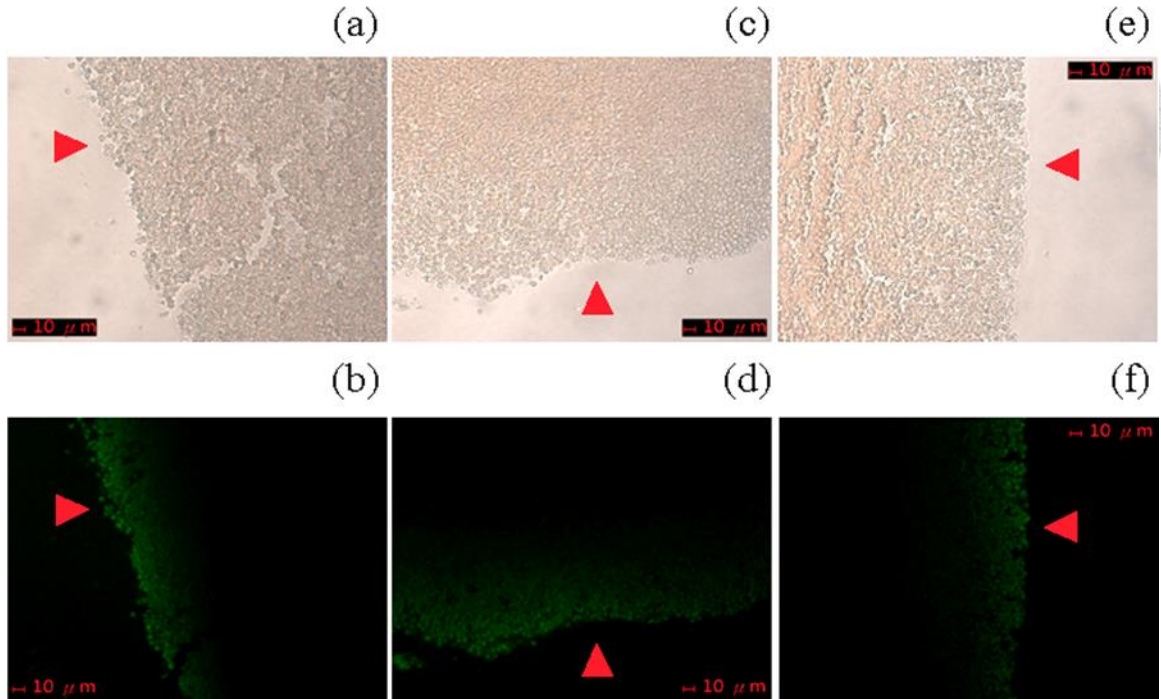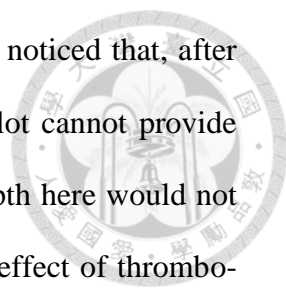
Fig. 12. Confocal microscopy photographs of blood clots. Upper and lower rows are in color and FITC fluorescence mode, respectively. Microbubble concentration is 8×10^6/ml. Red arrowheads indicate the clot surface. (a) and (b) are radiation force group. (c) and (d) are cavitation group. (e) and (f) are radiation force combined with cavitation group. The photographs in the same experimental group are from the same slice.

In order to quantify the fluorescence while minimizing observational bias, we converted the fluorescence images in Fig. 10–12 into 8-bit grayscale values (from 0 to 255) and then calculated the fluorescence intensity (as the difference between the region of interest and the average background) and depth (distance from clot surface traveled by the MBs). Fig. 13(a) shows an example of fluorescence curve sampled from the images in the lower panels of Fig. 10 that had been converted into grayscale images. Fig. 13(b) and 13(c) present the results of fluorescence calculation. The dashed line in Fig. 13(a) represents the calculated depth and the grayscale value used when calculating the average fluorescence intensity. The results of Fig. 13(b) and (c)

represent the distribution of avidin molecules within the clots. We noticed that, after possible thrombolysis presented in Fig. 9, the fallen part of the clot cannot provide fluorescence here. In other words, the fluorescent intensity and depth here would not be interpreted as another presentation of weight reduction or total effect of thrombolysis. The fluorescence intensity on the clot increased with the microbubble concentration in each type of experimental groups, as shown in Fig. 13(b) and (c) and statistically significant ($p<0.05$). Fig. 13(b) shows that the fluorescence intensities in the radiation-force group were 1.9, 2.5, and 4.4 times ($p<0.05$) higher than that in the control group for microbubble concentrations of 8×10^6/ml, 1.6×10^7/ml, and 4×10^7/ml, respectively, which was suggested by the total effect that active targeting of the avidin-biotin system assisted by the shear forces induced by the acoustic radiation forces. The corresponding fluorescence intensities in the cavitation group were 1.9, 3.5, and 4.2 times higher than that in the control group and statistically significant ($p<0.05$), which was explained by the shear forces associated with the effects of cavitation. Finally, the corresponding fluorescence intensities in the RF+Cav group were 1.6, 2.2, and 5.4 times higher than that in the control group and statistically significant ($p<0.05$), which was explained by the shear forces produced by radiation forces and cavitation. Note that the fluorescence depths are not comparable between the groups with different acoustic exposures and the same bubble concentration. However, MBs did travel further (typically by 10~20 μm) than in the control group after being exposed to radiation forces, cavitation, or both. Also the statistics are significant ($p<0.05$).
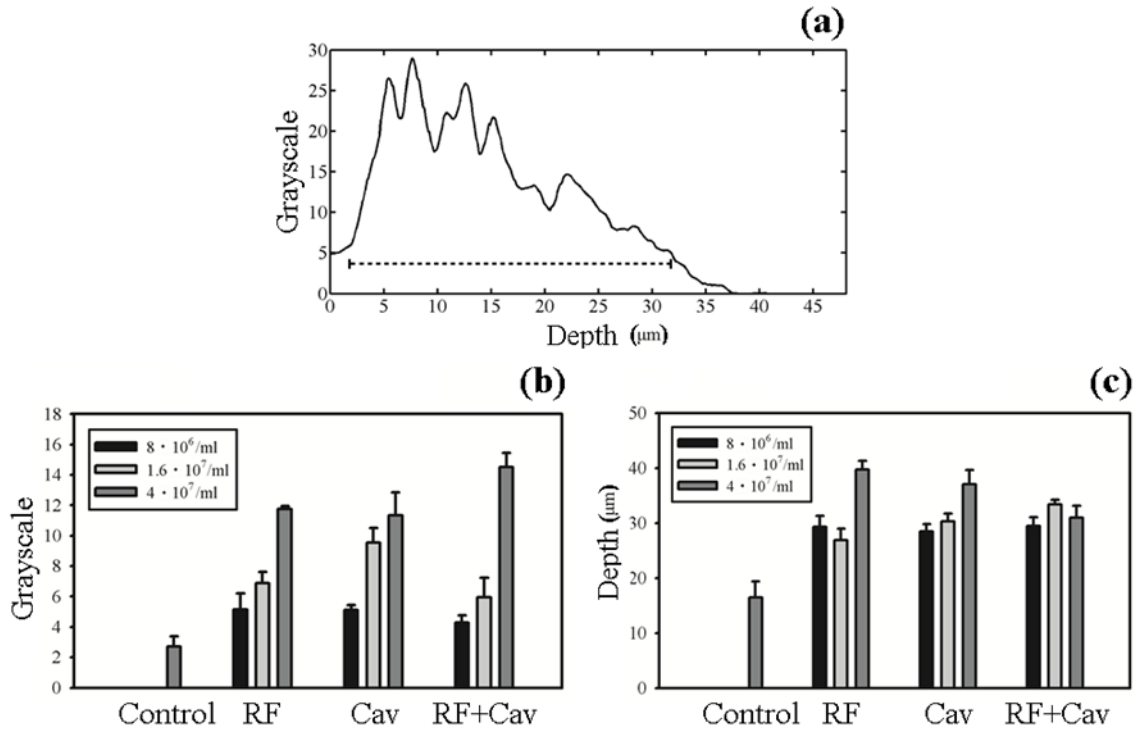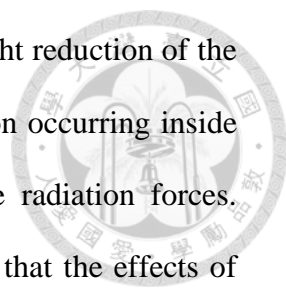
Fig. 13. Calculations about fluorescence intensity and distribution in depth. (a) Example fluorescence curve sampled from fluorescence images in Fig. 10, 11, 12 converted into grayscale values. The dashed line represents the calculated depth and the grayscale value used when calculating the average fluorescence intensity. (b) Average fluorescence intensity. (c) Fluorescence distribution in depth from clot surface. Data in panels b and c are mean and SD values.

3.4 Discussion

We have found that combining radiation forces with cavitation can reduce the damage to the surrounding tissue and improve the efficacy of sonothrombolysis. Cavitation-related tissue damage after microbubble destruction has been demonstrated at high doses of MBs and high acoustic pressures (greater than those used clinically) [129,130]. One possible way of reducing unwanted cavitation-induced tissue damage is to localize MBs to the target area. Our results in Fig. 9 demonstrate that combining

radiation forces with cavitation provided an additional 3–10% weight reduction of the thrombus relative to cavitation alone. We attribute this to cavitation occurring inside the blood clot after the targeting of MBs was enhanced by the radiation forces. Devcic-Kuhar et al. showed both theoretically and experimentally that the effects of radiation forces on sonothrombolysis are much less than those of microstreaming [131]. They used thrombolytic agent recombinant t-PA exposed to standing and travelling waves for their study and no microbubble was added. They concluded that acoustic streaming and shear stress are probably the most important mechanisms of ultrasound contributing to thrombolysis enhancement. In our experiments the radiation forces exerted minimal effects on thrombolysis with added MBs but without thrombolytic enzyme. However, combining radiation forces with cavitation effects produced an additional weight reduction of the thrombus relative to the cavitation group, with this being evident even for lower microbubble concentrations. These findings look promising for reducing the unwanted damage produced by cavitation when using radiation forces to enhance the targeting and localization of MBs.

Figs. 10–13 show that the MBs were distributed at greater depths (by 10~20 μm) in all of the experimental groups than in the control group. The microbubble distribution on the clot surface in the cavitation group are likely due to microjetting and microstreaming phenomena, while the shear forces produced by the radiation forces are suggested to explain the results obtained in the radiation-force group. Many previous studies have focused on the shear forces produced by radiation forces in a fluid [22,54–56]. Our results provide evidence that radiation forces can be used to enhance the movement and targeting of MBs inside tissues such as a thrombus. Such enhancement of targeting could be employed to deliver drugs across the leaky vessels in tumors and inflammatory tissues, as suggested by Hashizume et al. [132]. The spatial

selectivity provided by radiation forces has substantial potential to improve the localization of delivery and reduce systemic toxicity [133]. Nonspecific endothelium or vessel-wall damage produced by cavitation could also be reduced by localizing MBs using radiation forces [56,134–137]. The combined application of radiation forces and cavitation provides better effects in sonothrombolysis than do radiation forces or cavitation alone, as shown in Fig. 9.

3.5 Conclusions

Acoustic radiation forces facilitate the targeting of MBs to blood clots, and this study has demonstrated that combining radiation forces and cavitation provides better effects in sonothrombolysis than do radiation forces or cavitation alone.
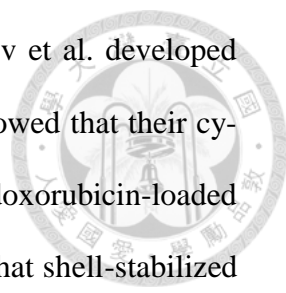
Chapter 4

Albumin Acts Like TGF-β1 in Microbubble-Based Delivery
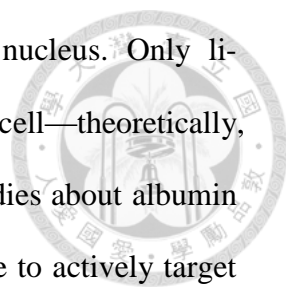
4.1 Introduction

Chemotherapy is one of the most important approaches for treating breast cancer patients. However, chemotherapeutic drugs such as paclitaxel (PTX) and doxorubicin lack cytotoxicity selectivity between cancer cells and normal cells, which frequently leads to serious side effects. Also, the poor water solubility of PTX makes it difficult to administer in clinical applications. Drug resistance and limited access of the drug often results in the drug concentration not been sufficiently high to kill malignant cancer cells [65, 66]. Therefore, localized drug delivery looks promising in reducing systemic toxicity and maximizing tumor exposure [67]. Drug-loaded-MBs destruction in combination with ultrasound has recently become one of the most promising therapeutic applications in drug delivery [68], since drug-loaded MBs can be manipulated and destroyed by ultrasound applied at the tumor site, causing localized release of the drug [69-72]. In addition, combining MBs with ultrasound can increase the permeability of physiologic barriers such as the blood–brain barrier, capillary endothelium, and the cell membrane for macromolecules or even colloidal particles [73, 74]. Several investigations on the application of ultrasound contrast agents as tumor drug delivery systems have recently been reported. Kang et al. showed an antitumor effect of docetaxel-loaded lipid-shelled MBs combined with ultrasound-targeted MB activation on VX2 rabbit liver tumors [75]. Xing et al. demonstrated the effective treatment of

ovarian carcinoma using PTX-loaded ultrasound MBs [76]. Tinkov et al. developed doxorubicin-loaded MBs with ideal physical characteristics and showed that their cytotoxic activity was enhanced relative to free doxorubicin and doxorubicin-loaded liposomes in in vitro experiments [77]. These studies have shown that shell-stabilized MBs can be used to load drugs or genes and improve the drug therapeutic index of a tumor when combined with ultrasound.
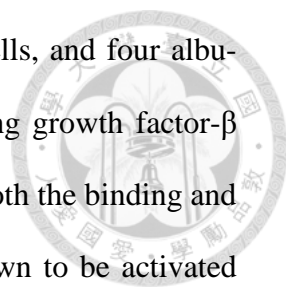
Acoustic cavitation refers to linear or nonlinear oscillations of gas and vapor cavities under the influence of an acoustic field [138]. The mechanical effects of acoustic cavitation and the interactions of MBs with biological media have been reported to play a key role in sonothrombolysis [114, 139-140], the increased and reversible permeability of the cell membrane and skin to large molecules (sonoporation) [141], reversible opening of the blood–brain barrier [142], and the release and delivery of genes for treating cardiovascular diseases [143, 144]. Ultrasound contrast agents provide a plentiful supply of cavitation nuclei [114], which substantially increases the probability of inducing cavitation. The shell can be constructed from various materials, including polymer, lipid, or protein. MBs can transport bioactive materials—such as drugs or genes incorporated on or within their shells—to a specific site within the body. MBs can transport drugs or materials into cells via different mechanisms. One is sonoporation of the cell membrane produced by microjetting of MBs under acoustic cavitation [145, 146]. MBs collapsing near a capillary or blood vessel wall may cause the liquid jet to penetrate the wall and cause extravasation [147]. Lipid-shelled MBs and albumin-shelled MBs can produce sonoporation effects under exposure to acoustic cavitation. Another mechanism is exchange or fusion of the phospholipid MB coating with the phospholipid bilayer of a cell membrane. This can deliver the cargo of the MB directly into the cytoplasm of the cell, with the possi-

bility of further uptake in endosomes or delivery to the cell nucleus. Only lipid-shelled MBs possess this ability to deliver drugs or DNA into a cell—theoretically, albumin MBs cannot enter cells through this mechanism. Most studies about albumin MBs have used antibodies that were conjugated on the MB surface to actively target antigens on the cell membrane. The third mechanism is endocytosis or phagocytosis by cells that may be involved in the uptake of whole MBs, MB fragments, or material entrapped in MBs [148]. Again, both lipid and albumin MBs can undergo this process with antigens or antibodies conjugated on their surfaces [147, 149-152]. Chemotherapeutic agents such as PTX can be incorporated into lipid MBs or albumin MBs or nanoparticles due to their lipophilic characteristic [153, 154]. Tumors and inflammatory tissues exhibit leaky vasculatures, meaning that the endothelial junctions are sufficiently porous to allow materials or MBs to pass. The endothelial gaps of tumor vessels can typically reach 380 to 780 nm [155]. Targeted MBs can be designed to bind specifically to cancer cells. Extravasation of MBs under exposure to acoustic cavitation or a radiation force helps targeted MBs to bind tumors and release drugs [147, 156-161].

One important therapeutic property associated with albumin MBs specifically is their increased adherence to damaged vascular endothelium. Albumin MBs do not adhere to normal endothelium, but they do adhere to activated endothelial cells or to the extracellular matrix of the disrupted vascular wall [162-164]. These interactions can be used not only for molecular imaging but also for therapeutic approaches in diseases such as atherosclerosis. This characteristic allows the delivery of drugs or genes bound to albumin MBs to be selectively concentrated at the site of vascular injury in the presence [164] or absence [165] of ultrasound application. Albumin has been shown to induce endocytosis in the endothelial cells lining vessel walls [166,

167]. Albumin endocytosis is extensively studied in endothelial cells, and four albumin-binding proteins have been described [168-171]. Transforming growth factor-β (TGF-β) receptors I and II (TβRI and TβRII) play crucial roles in both the binding and endocytosis of albumin. Subsequent signaling pathways were shown to be activated successfully [172, 173]. Two regions of sequence homology were found between albumin and TGF-β_1 that explain the binding interaction between albumin and TβRII [174]. The TGF-β superfamily is important due to elevated TGF-β being tumor-suppressive during early tumor outgrowth, whereas at later stages this switches to malignant conversion and progression [175, 176]. Loss of TGF-β growth inhibition and increased expression of TGF-β have been associated with malignant conversion and progression in breast cancer, as well as endometrial, ovarian, and cervical cancers [176, 177]. Elevated plasma TGF-β_1 levels in breast, lung, and prostate cancer patients are correlated with poor outcome [178]. All of these characteristics of albumin and TGF-β suggest that albumin MBs could play roles in cancer therapy.

Sollner and Bondy established that particles in suspension experience a force in the axial direction (the radiation force) in an acoustic field [179]. Two components of this radiation force, also known as the Bjerknes force, have been described: (1) a primary force, which is directed away from the source, and (2) a secondary force, which is typically attractive between ultrasound contrast MBs [180]. Dayton et al. verified that primary radiation forces were able to displace nontargeted MBs away from the vessel center *in vitro* and in the mouse microcirculation *in vivo*, and observed a concomitant reduction in the MB velocity [181]. Radiation-force-induced displacement results in strain that induces gaps between endothelial cells [159, 182] and widens intercellular spaces in epithelial tissue [157]. The application of an acoustic radiation force has been suggested for enhancing the delivery of therapeutic substances [183,

184]. Such localized delivery of MBs also has the potential to improve the safety and efficacy of sonothrombolysis induced by cavitation [185].

In the present study, we evaluated the interactions between an acoustic radiation force, cavitation, PTX-loaded albumin MBs, and MDA-MB-231 breast cancer cells. We further delineated the possible influences of TGF-β_1 and a radiation force on the behavior of cells and albumin MBs.

4.2 Materials & Methods

4.2.1 Microbubble Preparation

Albumin MBs were prepared with human albumin (Octapharma, Lachen, Switzerland) added to normal saline at 1.2%, ventilated with perfluoropropane, and sonicated (S-450D, Branson Ultrasonics, Danbury, CT, USA) at 280 W for 2 min, and then incubated on ice for 30 min. The concentration of the MBs was 8×10^9/mL, and they had diameters of 1.91±0.76 μm (mean±SD; Multisizer 3, Beckman Coulter, Fullerton, CA, USA), which changed by less than 1% after 3 hours at 4℃. The MB concentration in the experiments was 4×10^9/mL. Albumin MBs were mixed with avidin (Thermo Fisher Scientific, Rockford, IL, USA) combined with the albumin-saline solution at 0.04% [184]. We observed the interaction between MBs and cells during acoustic wave exposure in biotin-4-fluorescein (final concentration, 0.01%; AnaSpec, San Jose, CA, USA) mixed into the avidin-conjugated albumin MB solution and incubated at room temperature for 15 min while protected from light. These experiments showed that the binding between the fluorescent biotin and the avidin on the MBs produces fluorescent MBs, which makes them easy to locate under a confocal microscope.

Due to the poor solubility of PTX powder in water, it was dissolved in chloroform, emulsified by sonication, freeze-dried by liquid nitrogen, and added to normal saline to produce a suspension. PTX-loaded albumin MBs were manufactured by adding a PTX (LC Laboratories, Woburn, MA, USA) suspension into the solution to a concentration of 200 μM and using sonication as described above.

4.2.2 Cell Preparation

Cells of the MDA-MB-231 human breast cancer cell line were obtained from Professor Eric Y. Chuang (Chairman of Graduate Institute of Biomedical Electronics and Bioinformatics, National Taiwan University) and maintained with Leibovitz's L-15 medium (Gibco, Grand Island, NY, USA) in an incubator at 37℃ with no CO_2 added. Before ultrasound or reagent exposure, cells were harvested into 1.5-mL microcentrifuge tubes (Labcon, Petaluma, CA, USA) and kept sterile. After exposure, cells were transfer into 12-well culture plates (Becton Dickinson, Franklin Lakes, NJ, USA) and cultured for another 24 or 48 hours according to the experimental design.

4.2.3 Ultrasound System

The acoustic measurement setup is shown in Figure 14. A 1.0-MHz transducer (V302, Panametrics-NDT, Waltham, MA, USA) with a diameter of 25.4 mm and a focal length of 49.8 mm was used for transmission. The transmitted waveforms were generated by a digital-to-analog converter (CompuGen 1100, GaGe Applied Technologies, Lachine, QC, Canada) and amplified by a power amplifier (250A250A, Amplifier Research, Souderton, PA, USA). The acoustic signals were detected by an unfocused 10-MHz transducer (V312, Panametrics-NDT) and sent to a receiver (5072PR, Panametrics-NDT). Pulsed waves were used in this study with a repetition

frequency of 100 Hz, pulse duration of 50 cycles, and acoustic pressures of about 1.32 MPa for inducing cavitation [139]. A radiation force was applied using a pulsed wave with a repetition frequency of 100 Hz, pulse duration of 100 cycles, and acoustic pressure of 0.12 MPa. During experiments, the radiation force and cavitation exposure were repeated 50 and 20 times, respectively, at each stimulus level to increase their effects on cells [185]. The radiation force and cavitation exposure were combined by applying an acoustic radiation force followed by cavitation, and repeatedly alternating them for their respective durations to allow accurate comparisons. A 2% agarose phantom was constructed with a cylindrical cavity (11 mm in diameter) to hold the microcentrifuge tube. Both transducers were positioned with their focuses within the cavity.
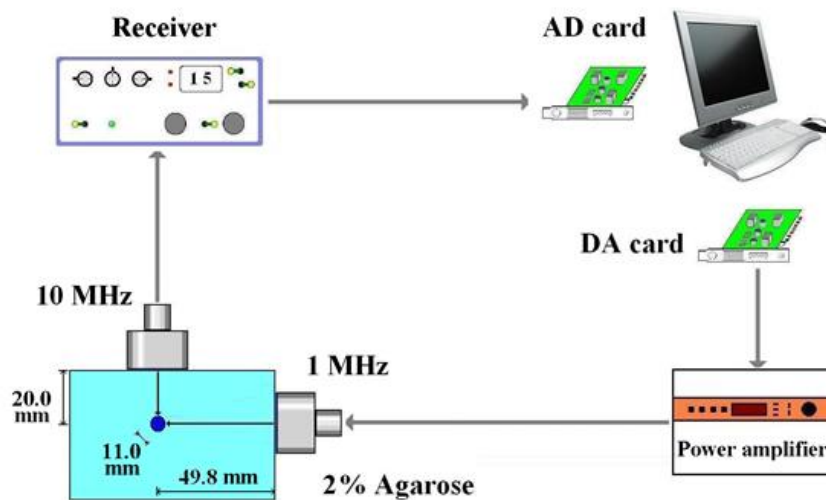

Figure 14. Setup for acoustic stimulation.

4.2.4 Flow Cytometry Examination

Cell apoptosis was assessed by the FITC Annexin-V Apoptosis Detection Kit (BD Pharmingen, San Diego, CA, USA) according to the manufacturer's recommendations. The proportion of stained annexin-V cells was determined by a flow cytome-
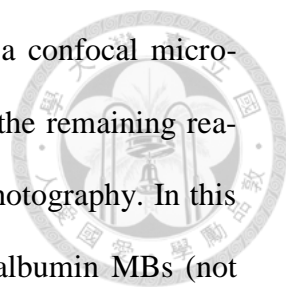
ter (FACSCalibur, BD Bioscience, San Jose, CA, USA) and analyzed by free software (WinMDI version 2.9).

4.2.5 Study Protocol

We first evaluated the interaction between cells and PTX-loaded albumin MBs under different acoustic stimuli based on the cell apoptosis rate. With PTX-loaded MBs (final PTX concentration, 100 μM) added into the cell suspension, acoustic waves for inducing a radiation force or cavitation were applied, alone or in combination, in different experimental groups. Sham treatments involved exposing cells (1) to albumin MBs without applying drugs or acoustic stimulation, (2) to PTX-loaded albumin MBs without acoustic stimulation, and (3) to a PTX suspension (final concentration, 100 μM) without acoustic stimulation. The control group comprised cells exposed to no MBs, PTX, or acoustic waves. After performing these procedures the cells were incubated for 48 hours to allow apoptosis to occur, and then examined by flow cytometry. This experiment was repeated three times to obtain reliable values of the apoptosis rate.

We then used by confocal microscopy to evaluate the interactions between cells, albumin MBs, TGF-β1, and an acoustic radiation force. Fluorescent MBs were mixed with the cell suspension and exposed to an acoustic radiation force. In another experimental group the cells were treated with TGF-β1 (PeproTech, Rocky Hill, NJ, USA) as a blocking assay to a final concentration of 0.05 ng/ml for 30 min at 37℃ before the application of fluorescent MBs and acoustic waves. Other groups included cells exposed to fluorescent MBs, cells treated with PTX-loaded fluorescent MBs, cells treated with biotin-4-fluorescein solution (not in the form of MBs), and cells exposed to nothing (as in the control). After these experimental procedures, cells were

divided into two major groups: (1) immediate observation under a confocal microscope and (2) incubation for 24 hours followed by washing away the remaining reagents by normal saline and examination under a microscope and photography. In this case we simplified our experimental model by using fluorescent albumin MBs (not PTX-loaded fluorescent AMBs) to observe the MB–cell interaction. Sterile coverslips were put into culture plates for cells to adhere and help transfer onto glass slides for confocal microscope examination (TCS SP2, Leica Microsystems, Heidelberg, Germany). In each experimental group, at least 800 cells were calculated and recorded from in at least 5 visual fields on the same glass slide in order to minimize observation bias. These experiments were also repeated three times, with consistent results obtained each time.

4.2.6 Statistics

The obtained results are given here as mean and standard deviation values and compared using the Kruskal-Wallis test. A probability value of $p < 0.05$ was considered statistically significant.

4.3 Results

Figure 15 shows the cell apoptosis results after exposure to PTX-loaded albumin MBs, a radiation force, and cavitation. Figure 16 summarizes the apoptosis rates for these experiments. Comparing the experimental groups in Figures 15 and 16 reveals that the presence of PTX-loaded MBs in the cell medium increased the apoptosis rate by 2.4% ($p < 0.05$) relative to MBs without PTX. Applying either an acoustic radiation force or cavitation alone to cells with PTX-loaded MBs increased the apoptosis

rate to 12.1% and 15.2% ($p < 0.05$), respectively, relative to PTX-loaded MBs. Applying a radiation force and cavitation alternately produced an apoptosis rate of 31.3% ($p < 0.05$), which is higher than that for radiation force or cavitation alone. The PTX-drug-suspension group reached an apoptosis rate of 53.8% ($p < 0.05$) without acoustic stimulation. However, the apoptosis rate in the PTX-loaded-MBs group was 11.1% ($p < 0.05$). This can be explained by some of the drug molecules forming MBs while others remain in suspension during the process of sonication to form PTX-loaded MBs, and the efficacy of PTX reducing due to a temperature increase. The MBs group with an 3.7% ($p < 0.05$) increase in the apoptosis rate, relative to the control group, showed the background influence of MBs on cell apoptosis.
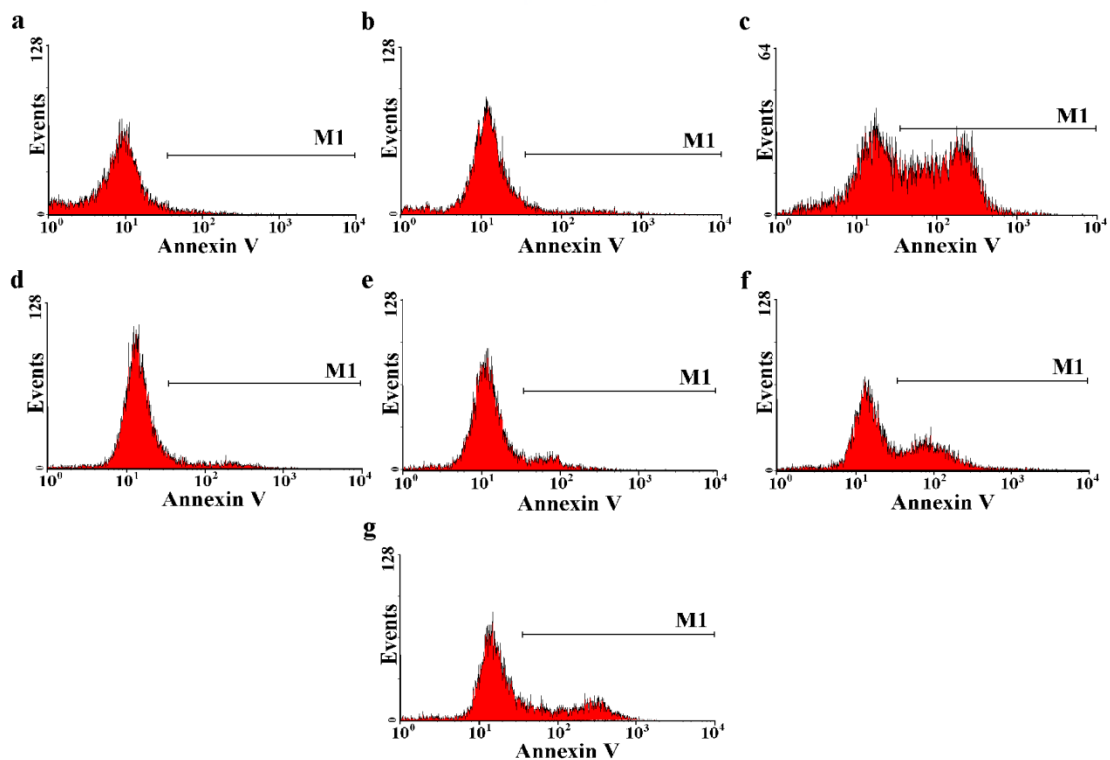

Figure 15. Flow cytometry results of cell apoptosis after applying PTX-loaded MBs, an acoustic radiation force, and cavitation: (a) control, (b) albumin-shelled MBs only, (c) PTX only, (d) PTX-loaded albumin MBs, (e) a radiation force and PTX-loaded albumin MBs, (f) cavitation and PTX-loaded albumin MBs, and (g) a radiation force, cavitation, and PTX-loaded albumin MBs.
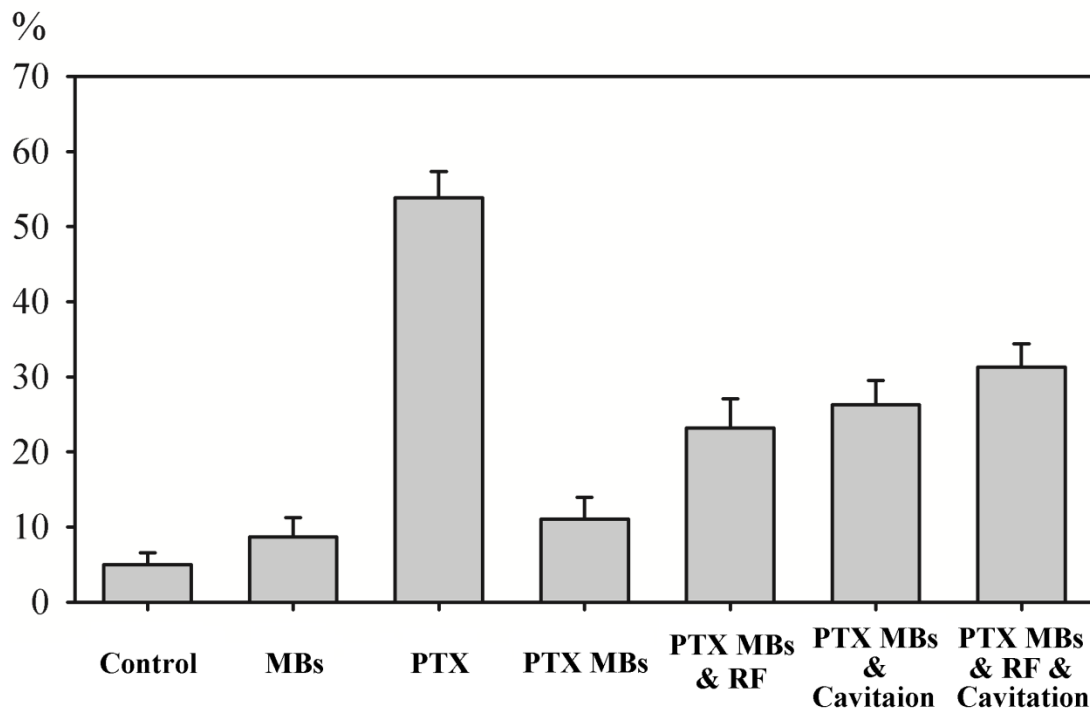
Figure 16. Statistics results of the cell apoptosis rate from flow cytometry. The mean percentage of annexin-V-positive cells from individual experiments is shown for each condition. Error bars indicate standard deviations. RF, radiation force.

Figure 17 presents photographs of the interactions between cells, albumin MBs, TGF-β1, and the acoustic radiation force taken immediately after the experiments; Figure 18 shows the corresponding photographs taken 24 hours after the experiments. Figure 17b shows that fluorescent MBs did not enter cells immediately after being added into the cell suspension, as in the control group in Figure 17a (none of cells in either group exhibited fluorescence). Figure 17c shows that fluorescent MBs entered cells immediately after exposure to an acoustic radiation force. Fluorescent MBs were present in 15.9% (p < 0.05) of the cells. However, after incubation of TGF-β1 with cells followed by exposure to an acoustic radiation force, none of the cells contained fluorescent MBs in our experiment, as shown in Figure 17d.

Figure 18c demonstrates that many more cells contained fluorescent MBs after 24 hours of incubation (70.5%, $p < 0.05$), indicating that cells can uptake fluorescent MBs spontaneously during incubation. Figure 18b shows that cells did not uptake biotin-4-fluorescein in solution form, resulting in low background fluorescence. Fluorescence was exhibited by 55.6% ($p < 0.05$) of the cells in Figure 18d. This group demonstrates that PTX-loaded albumin MBs can enter the cells without the application of an acoustic radiation force or cavitation. Comparison of Figure 18e with Figure 18c shows that exposures to a radiation force increased the proportion of cells containing fluorescent MBs to 91.9% ($p < 0.05$). However, incubation of TGF-β1 decreased this proportion to 0%, as shown in Figure 18f and 18g. The effect exerted by radiation force on cell uptake disappeared after introducing TGF-β1 in the experiments. Figure 19 delineates the distribution of fluorescent MBs inside the cells.
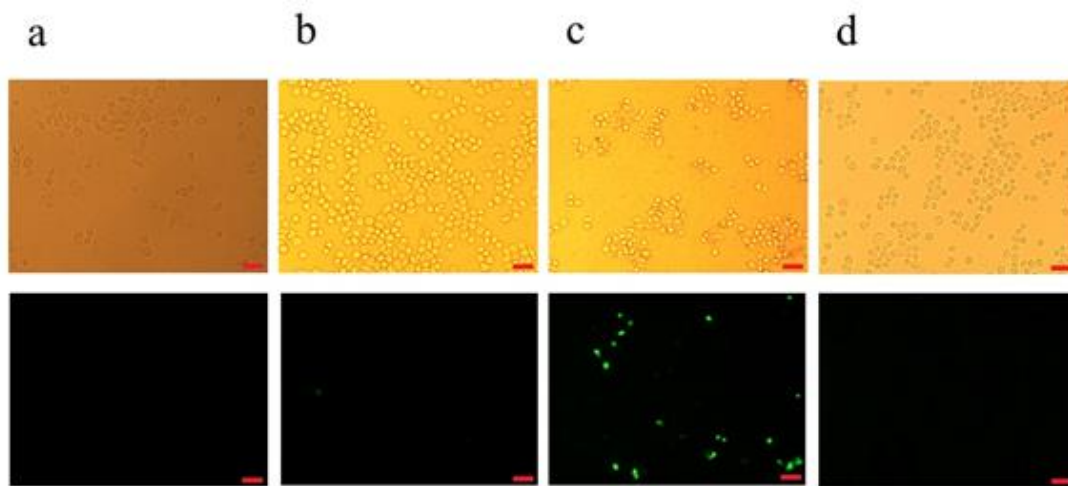

Figure 17. Microscopy images (100× magnification) of microbubble-cell interactions immediately after radiation force and TGF-β1 application: (a) Control, (b) Fluorescent MBs only, (c) Fluorescent MBs and radiation force, (d) TGF-β1, fluorescent MBs, and radiation force. Upper row of photography is in bright field, while lower row is in FITC fluorescence mode. Annexin V in figures means the intensity of staining. Scale Bar represents 50 um.
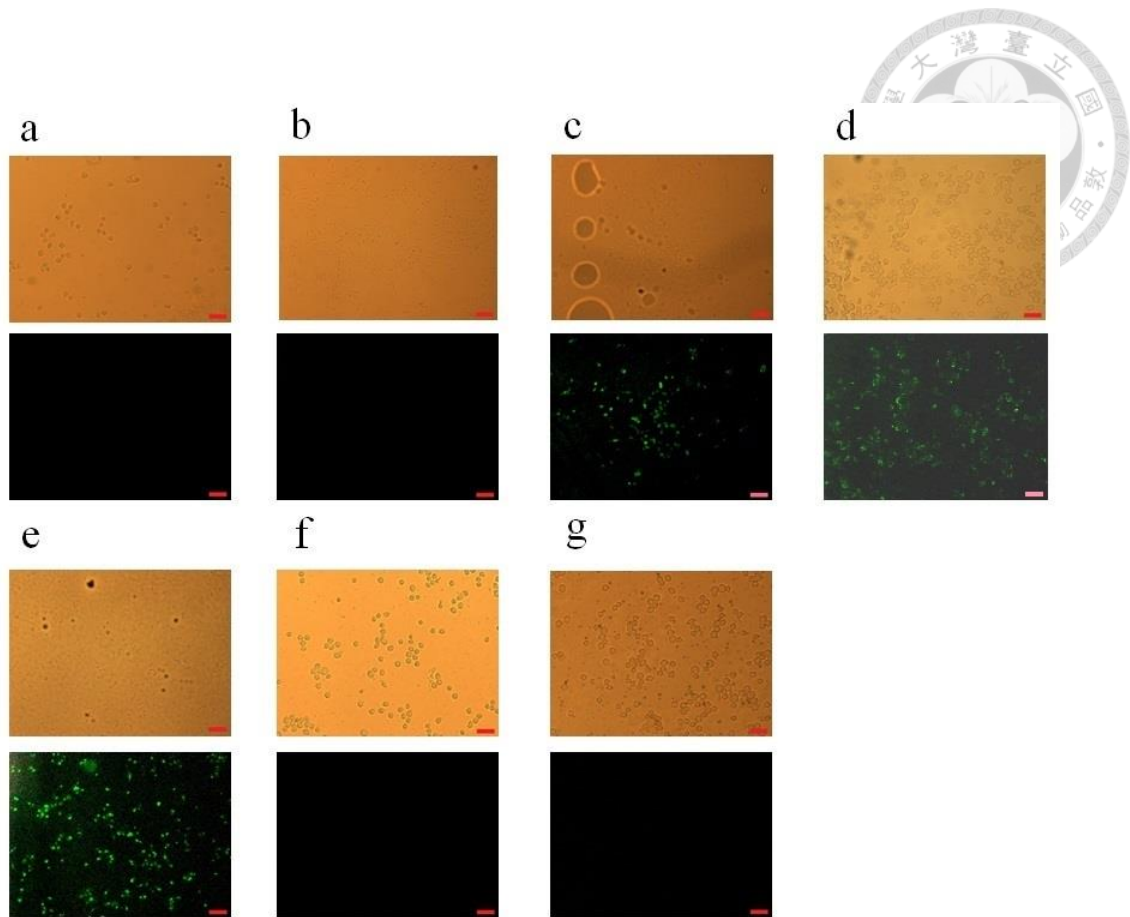
57

Figure 18. Microscopy images (100× magnification) of microbubble-cell interactions 24 hour after radiation force and TGF-β1 application: (a) Control, (b) Fluorescent agent (biotin-4-fluorescein) only, (c) Fluorescent MBs, (d) PTX-loaded fluorescent MBs, (e) Fluorescent MBs and radiation force, (f) TGF-β1 and fluorescent MBs, (g) TGF-β1, fluorescent MBs, and radiation force. Upper row of photography is in bright field, while lower row is in FITC fluorescence mode. Annexin V in figures means the intensity of staining. Scale Bar represents 50 um.
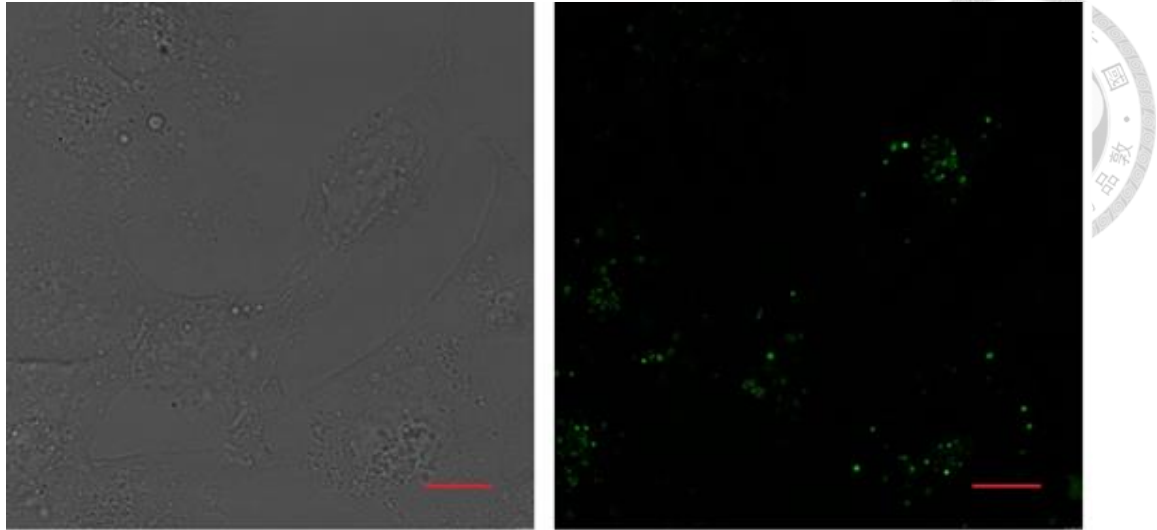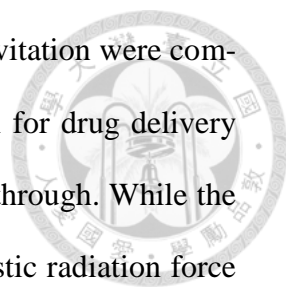
Figure 19. Microscopy images of fluorescent MBs inside breast cancer cells in 1000× magnification. Left photography is in bright field, and right one is in FITC fluorescence mode. Scale Bar represents 10 um.
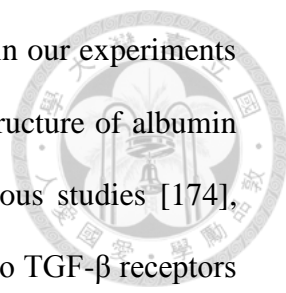
4.4 DISCUSSION

In this study we discovered that albumin MBs loaded with PTX can induce apoptosis in breast cancer cells. The use of an acoustic radiation force and cavitation appears to be a promising approach for inducing cell apoptosis effects, especially when these modes of stimulation are applied alternately. Albumin MBs entered breast cancer cells and remained therein for at least 24 hours, even in the presence of PTX loading, and applying an acoustic radiation force enhanced the endocytosis of MBs into cells. The interaction between albumin MBs and breast cancer cells can be blocked by TGF-β1, even with the assistance of an acoustic radiation force.

From the flow cytometry results shown in Figures 15 and 16, we concluded that an acoustic radiation force and cavitation increase the apoptosis rate of MDA-MB-231 cells in the presence of PTX-loaded albumin MBs. The apoptosis rate

of 5% was increased by a further 5% when a radiation force and cavitation were combined alternately. The mechanism underlying the use of cavitation for drug delivery involves creating holes in the cell surface that allow drugs to pass through. While the isotropic character of cavitation remains a major problem, an acoustic radiation force that pushes MBs away from the transducer provides a possible solution. The experimental results in Figure 15e show that this radiation force increased the probability of interactions between PTX-loaded MBs and cells, and increased the apoptosis rate to 23.2%. This force probably increased the local concentration of MB around the cells [186, 187]. Another explanation is that it influenced the behavior of receptors (increased cell uptake) and the cell membrane potential (hyperpolarization) [148, 188-189]. This proposed phenomenon explains the results shown in Figure 18g. Inducing cavitation after exerting a radiation force delivered more MBs into cells, increasing the apoptosis rate by 5% relative to the cavitation-alone group. However, the MBs used in the experiments contained no specific ligands or antibodies, only albumin molecules. A local increase in the concentration cannot fully explain the apoptosis rate in the radiation-force-alone group, since radiation force theoretically kills no cells. A possible explanation is that PTX-loaded MBs somehow entered the cells and released the drug. We therefore designed experiments to evaluate the interactions between cells, albumin MBs, TGF-β1, and an acoustic radiation force using confocal microscopy.

Figures 17 and 18 demonstrate that cells can uptake albumin MBs, including when they contain drugs. However, this process takes hours (comparing Figures 17b and 18c), but it is noticeably enhanced by applying an acoustic radiation force (Figures 17e and 18c). When a sufficient amount of TGF-β1 is added to bind all TGF-β receptors, the process of cell uptake is blocked. The spontaneous uptake by cells and

increased uptake of cells induced by a radiation force disappeared in our experiments (Figures 17d, 18f, and 18g). This could be due to the molecular structure of albumin being similar to that of the TGF-β family, as suggested by previous studies [174], which might allow albumin to act like a TGF-β molecule and bind to TGF-β receptors on the cell membrane. How tumor cells uptake albumin and the subsequent signal transduction have not been fully understood until now. Cells like vascular endothelium uptake albumin through four albumin-binding proteins and TβRI and TβRII [168-171]. The expression condition of albumin-binding proteins in breast cancer cells remains unknown. However, our experiments using a human breast cancer cell line demonstrated that TGF-β receptors are involved in albumin MB endocytosis. Albumin MBs that carried PTX also were successfully transported into tumor cells in our experiments. The application of an acoustic radiation force to assist the uptake of albumin MBs by cells therefore looks promising. However, it remains necessary to elucidate the uptake mechanism and mode of signal transduction.

Elevated TGF-β is tumor-suppressive during early tumor outgrowth, and cancer cells down-regulate the expression of TGF-β receptors. The loss of TGF-β growth inhibition and increased expression of TGF-β have been associated with malignant conversion and progression in breast cancer, as well as in endometrial, ovarian, and cervical cancers. At this stage, TGF-β receptors are up-regulated to become more sensitive to the stimulation of TGF-β that facilitates tumor growth. Since elevated plasma TGF-β1 levels in breast, lung, and prostate cancer patients are correlated with poor outcome, PTX-loaded albumin MBs are suitable for tumors in an advanced stage. First, the albumin molecules on MBs aid the adherence to damaged endothelium and extracellular matrix, or extravasate through tumor vessels. Second, primary and metastatic tumors can be visualized using ultrasonography after endocytosis of albumin

MB by tumor cells. Third, further application of an acoustic radiation force and cavitation would enhance local drug delivery into tumor cells. In an advanced tumor stage the endocytosis of albumin MBs by tumor cells would be expected to be elevated. Further animal studies of the efficacy and behaviors of PTX-loaded albumin MBs on tumor cells are indicated.

In Figure 3, PTX suspension group and PTX-loaded albumin MBs group showed significance difference in apoptosis rate. Our explanation is that the contact conditions between PTX molecules and cells are different in these two experimental groups. Some part of PTX molecules were loaded on MBs that makes contact chance changed. In our experiments we applied PTX at a concentration of 100 μM to the cells [189,190]. The concentration was determined in order to demonstrate that PTX molecules either loaded on MBs or in suspension still possess the pharmacologic effects to induce apoptosis. However, the decrease of pharmacologic effects of PTX cannot be ruled out during the manufacturing process.

In our study we used TGF-β1 to visualize the interaction between albumin MBs and breast cancer cells. However, the albumin molecule can interact with TβRI and TβRII [173], and other members of the TGF-β superfamily can potentially influence the interaction between albumin MBs and breast cancer cells. Further researches are indicated to understand the possible roles of the TGF-β superfamily in the endocytosis of albumin MBs and the pharmacologic behavior of PTX in MB form.

4.5 Conclusions

In this study we found that albumin MBs loaded with PTX induce breast cancer cell apoptosis. An acoustic radiation force and cavitation could induce apoptosis, es-

pecially when the two types of stimulation were applied alternately. Albumin MBs can enter breast cancer cells and remain therein for at least 24 hours, even in the presence of PTX loading. The application of an acoustic radiation force enhances the endocytosis process of MBs. The interaction between albumin MBs and breast cancer cells can be blocked by TGF-β1, even with the assistance of an acoustic radiation force. In our experiments we found that the entry of albumin MBs into breast cancer cells is mediated by TGF-β1 receptors.
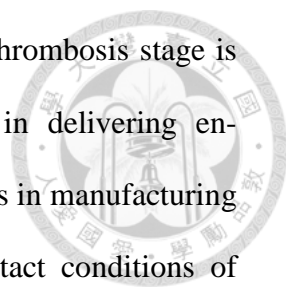
Chapter 5

Discussion, Conclusion & Future Work

5.1 Discussion

Our researches demonstrate that acoustic radiation force and cavitation play important roles in sonothrombolysis and drug delivery. Radiation forces can be used to enhance the localization and targeting of MBs to blood clots or breast cancer cells. Acoustic cavitation produces sonothrombolysis alone or in combination with thrombolytic enzymes. Combining these two acoustic waves produce synergistic effects in sonothrombolysis and PTX-loaded MBs induced apoptosis.

In our studies about enzymatic sonothrombolysis, we concluded that combining ultrasound, MBs, and thrombolytic agent is a promising method. The ICD we proposed is a useful indicator of thrombolysis. Thrombolysis produced by streptokinase treatment and cavitation showed synergistic effects. We also found that combining radiation forces with cavitation can reduce the damage to the surrounding tissue and improve the efficacy of sonothrombolysis. Radiation forces can be used to enhance the movement and targeting of MBs inside tissues such as thrombus. Such enhancement of targeting could be employed to deliver drugs across the leaky vessels in tumors and inflammatory tissues. The spatial selectivity provided by radiation forces has substantial potential to improve the localization of delivery and reduce systemic toxicity. The combined application of radiation forces and cavitation provides better effects in sonothrombolysis. According to our conclusions about sonothrombolysis, we suggest that radiation force looks promising in enhancing thrombolytic enzyme

delivery into blood clot. Since the structure of thrombus in early thrombosis stage is less compact than in late stage, radiation force is promising in delivering enzyme-conjugated MBs into blood clot. According to our experiences in manufacturing PTX-loaded albumin MBs, we expect that the efficacy and contact conditions of thrombolytic enzymes with thrombus would change after being loaded to MBs. This is important information when designing MBs for sonothrombolysis.

Another opinion comes from the effect that cavitation increases membrane or physiologic barrier permeability. In our studies, we concluded that the use of acoustic radiation force and cavitation appears to be a promising approach for inducing cell apoptosis effects, especially when these modes of stimulation are applied alternately. Further studies are indicated in applying radiation force for drug delivery after increases the barrier permeability. Another study approach is to apply cavitation to widen endothelium gaps in tumor vessels.

Previous studies suggest that MBs enter cells through endocytosis or phagocytosis mechanisms. Our study demonstrated that albumin MBs do enter breast cancer cells and blocked by TGF-β1 receptors. Albumin molecule has been found to be endocytosed by endothelium and transported to surrounding environments (transendothelial transport). However, endocytosis and signal transduction pathways belong to different cell functions. The roles of albumin molecule for cell functions remain unclear. How the albumin MB enters cell also remains an important question. The involvement of clathrin molecules in this process and the possible influences provided by radiation force need further delineation. The fate of albumin MBs after entering cells and its possible interactions with TGF-β signal transduction pathway are important issues as well.

5.2 Conclusions

The spatial selectivity provided by radiation forces has substantial potential to improve the localization of delivery and reduce systemic toxicity. Combining acoustic radiation force and cavitation produce synergistic effects in sonothrombolysis and PTX-loaded MBs induced apoptosis. The use of acoustic radiation force and cavitation appears to be a promising approach for inducing cell apoptosis effects, especially when these modes of stimulation are applied alternately. Our study demonstrated that albumin MBs do enter breast cancer cells and blocked by TGF-β1 receptors.

5.3 Future Works

In studies of sonothrombolysis, it is interesting to apply radiation force to deliver enzymes-conjugated MBs into blood clot. The degree of local concentration increase provided by radiation force remains unclear.

After increasing the physiologic barrier permeability by cavitation, the efficiency of drug delivery through the barrier provided by radiation force has not been evaluated. In blood vessels with relatively small endothelium gaps, cavitation can be applied to widen the gaps and increase drug delivery.

How the albumin MB enters cell remains an important question. The involvement of clathrin molecules in this process and the possible influence provided by radiation force needs further delineation. Another issue comes from the possible influence of drug-loaded albumin MBs in different stages of cancer. The fate of albumin MBs after entering cells and its possible interactions with TGF-β signal transduction pathway are important issues as well.

References:

1. Wells PNT. Biomedical ultrasonics. London: Academic Press, 1977.

2. Goldberg BB. Abdominal ultrasonograph. London: John Wiley & Sons, 1984.

3. Lewin PA, Goldberg BB. Ultrasound bioeffects for the perinatologist. In: Sciarra JJ, eds. Gynecology and obstetrics. Philadelphia: Lippincott-Ravan Publishers, 1997:1-18.

4. Stewart HD, Stewart HF, Moore RM Jr, Garry J. Compilation of reported biological effects data and ultrasound exposure levels. J. Clin. Ultrasound 1985;13(3):167-186.

5. Ziskin MC, Peitti DB. Epidemiology of human exposure to ultrasound: a critical review. Ultrasound Med Biol 1988;14:91-96.

6. Barnett SB, ter Haar GR, Ziskin MC, Maeda K. The sensitivity of biological tissue to ultrasound. Ultrasound Med Biol 1997;23:805-812.

7. Thomenius KE. Estimation of the potential for bioeffects. In: Ziskin MC, Lewin PA, eds. Ultrasonic exposimetry. Boca Raton, FL: CRC Press, 1993:371-407.

8. Apfel RE. Possibility of microcavitation from diagnostic ultrasound. IEEE Trans UFFC 1986;33:139-141.

9. Atchley AA. The blake threshold of a cavitation nucleus having a radius-dependent surface tension. J Acoust Soc Am 1988;85:152-157.

10. Holland CK, Apfel RE. Thresholds for transient cavitation produced by pulsed ultrasound in a controlled nuclei environment. J Acoust Soc Am 1990;88:2059-2069.

11. Madanshetty SI, Roy RA, Apfel RE. Acoustic microcavitation: its active and passive acoustic detection. J Acoust Soc Am 1991;90:1515-1526.

12. Deng CX, Xu Q, Apfel RE, Holland CK. In vitro measurements of inertial cavi-

tation thresholds in human blood. Ultrasound Med Biol 1996;22:939-948.

13. Crum LA. Nucleation and stabilization of MBs in liquids. Appl Sci Res 1982;38:101-115.

14. Atchley AA, Crum LA. Acoustic cavitation in bubble dynamics in Ultrasound: Its chemical, physical, and biological effects. New York: K. S. Suslick, VCH Publishers,1988:64.

15. Ivey JA, Gardner EA, Fowlkes JB, Rubin JM, Larson PL. Acoustic generation of intra-arterial contrast boluses. Ultrasound in Med & Biol 1995;21:757-767.

16. Ophir J, Parker KJ. Contrast agents in diagnostic ultrasound. Ultrasound Med Biol 1989;15:319-325.

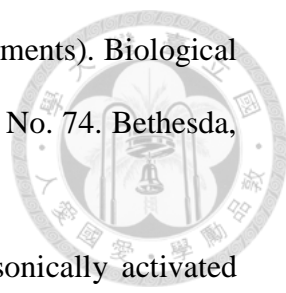17. de Jong N. Improvements in ultrasound contrast agents. IEEE Eng Med Biol Mag 1996;15:72-82.

18. Goldberg BB. Ultrasound contrast agents. London: Martin Dunitz Ltd., 1997.
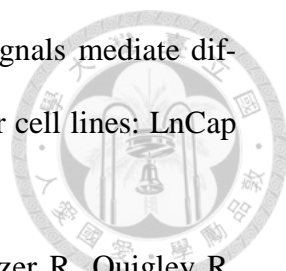
19. Borden MA, Kruse DE, Caskey CF, Zhao S, Dayton PA, Ferrara KW. Influence of lipid shell physiochemical properties on ultrasound-induced microbubble destruction. IEEE Trans UFFC 2005;52(11):1992-2002
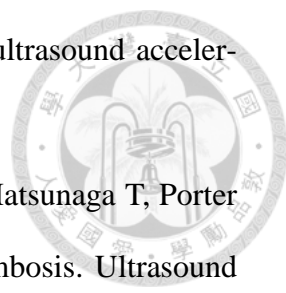
20. Porter TR, Xie F. Transient myocardial contrast after initial exposure to diagnostic ultrasound pressures with minute doses of intravenously injected MBs. Circulation 1995;92:2391-2395.

21. Shi WT, Forsberg F, Oung H. Spectral broadening in conventional and harmonic Doppler measurements with gaseous contrast agents. Proc IEEE Ultrason Sympos 1997:1575-1578.
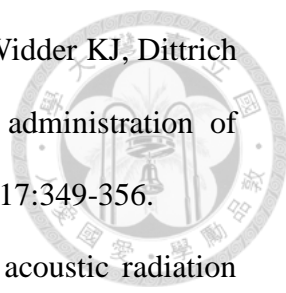
22. Dayton PA, Morgan KE, Klibanov AL, Brandenburger GH, Ferrara KW. Optical and acoustical observations of the effects of ultrasound on contrast agents. IEEE Transaction UFFC 1999;46:220-232.

23. NCRP (National Council on Radiation Protection and Measurements). Biological effects of ultrasound: Mechanisms and clinical implications Report No. 74. Bethesda, MD: NCRP, 1983.

24. Miller DL. Particle gathering and microstreaming near ultrasonically activated gas-filled micropores. J Acoust Soc Am 1988;84:1378-1387.

25. Kondo T, Kodaira T, Kano E. Free radical formation induced by ultrasound and its effects on strand breakage in DNA of cultured FM3A cells. Free Rad Res Comm 1993;19:S193-S200.

26. Chen WS, Brayman AA, Matula TJ, Crum LA. Inertial cavitation dose and hemolysis produced in vitro with or without Optison®. Ultrasound Med Biol 2003;29:725-737.

27. Cramer E, Lauterborn W. Acoustic cavitation noise spectra. Appl Sci Res 1982;38:209-214.

28. Everbach EC, Makin IRS, Azadniv M, Meltzer RS. Correlation of ultrasound-induced hemolysis with cavitation detector output in vitro. Ultrasound Med Biol 1997;23:619-624.

29. Lauterborn W, Cramer E. On the dynamics of acoustic cavitation noise spectra. Acustica 1981;49:280-287.

30. Kruse DE, Yeh CK, Ferrara KW. A new imaging strategy utilizing wideband transient response of ultrasound contrast agents. Honolulu, HI: IEEE. Ultrasonics Symposium 2003;1:424-428.

31. Bao S, Thrall BD, Miller DL. Transfection of a reporter plasmid into cultured cells by sonoporation in vitro. Ultrasound Med Biol 1997;23:953-959.

32. Kim HJ, Greenleaf JF, Kinnick RR, Bronk JT, Bolander ME. Ultrasound-mediated transfection of mammalian cells. Hum Gene Ther 1996;7:1339-1346.

33. Tata DB, Dunn F, Tindall DJ. Selective clinical ultrasound signals mediate differential gene transfer and expression in two human prostate cancer cell lines: LnCap and PC-3. Biochem Biophys Res Commun 1997;234:64-67.

34. Unger EC, Matsunaga TO, McCreery T, Schumann P, Sweitzer R, Quigley R. Therapeutic applications of MBs. Eur J Radiol 2002;42:160-168.

35. Van Wamel A, Bouakaz A, de Jong N. Duration of ultrasound bubbles enhanced cell membrane permeability. Honolulu, HI: IEEE. Ultrasonics Symposium 2003;1:917-920.

36. Wyber JA, Andrews J, D'Emanuele A. The use of sonication for the efficient delivery of plasmid DNA into cells. Pharm Res 1997;14:750–756.

37. Unger EC, Hersh E, Vannan M, Matsunaga TO, McCreery T. Local drug and gene delivery through MBs. Prog. Cardiovasc Dis. 2001;44(1):45-54.

38. Culp WC, McCowan TC. Ultrasound Augnmented Thrombolysis. Current Medical Imaging Review 2005;1:5-12.

39. Molina CA, Ribo M, Rubiera M, Montaner J, et al. Microbubble administration accelerates clot lysis during continuous 2-MHz ultrasound monitoring in stroke patients treated with intravenous tissue plasminogen activator. Stroke 2006;37(2):425-429.

40. Trubestein G, Engel C, Etzel F, Sobbe A, Cremer H, Stumpff U. Thrombolysis by ultrasound. Clin Sci Mol Med 1976;3:697s-698s.

41. Everbach E, Francis C. Cavitational mechanisms in ultrasoundaccelerate thrombolysis at 1 MHz. Ultrasound Med Biol 2000;26:1153-1160.

42. Datta S, Coussios CC, McAdory LE, Tan J, Porter T, de Courten-Myers G, Holland CK. Correlation of cavitation with ultrasound enhancement of thrombolysis. Ultrasound Med Biol 2006;32(8):1257-1267.

43. Prokop AF, Soltani A, Roy RA. Cavitational mechanisms in ultrasound accelerated fibrinolysis. Ultrasound Med Biol 2007;33(6):924-933.

44. Xie F, Tsutsui JM, Lof J, Unger EC, Johanning J, Culp WC, Matsunaga T, Porter TR. Effectiveness of lipid MBs and ultrasound in declotting thrombosis. Ultrasound Med Biol 2005;31(7):979-985.

45. Mornstein V. Cavitation-induced risks associated with contrast agents used in ultrasonography. Eur J Ultrasound 1997;5:101-111.

46. Shi WT, Forsberg F. Ultrasonic characterization of the nonlinear properties of contrast MBs. Ultrasound Med Biol 2000;26:93-104.

47. Bailey MR, Dalecki D, Child SZ, Raeman CH, Penney DP, Blackstock DT, Carstensen EL. Bioeffects of positive and negative acoustic pressure in vivo. J Acoust Soc Am 1996;100:3941-3946.

48. Brayman AA, Miller MW. Acoustic cavitation nuclei survive the apparent ultrasonic destruction of Albunex microspheres. Ultrasound Med Biol 1997;23:793-796.

49. Dalecki D, Raeman CH, Child SZ, Cox C, Francis CW, Meltzer RS, Carstensen EL. Hemolysis in vivo from exposure to pulsed ultrasound. Ultrasound Med Biol 1997;23:307-313.

50. Dalecki D, Raeman CH, Child SZ, Penney DP, Carstensen EL. Remnants of Albunex nucleate acoustic cavitation. Ultrasound Med Biol 1997;23:1405-1412.

51. Dalecki D, Raeman CH, Child SZ, Penney DP, Mayer R, Carstensen EL. The influence of contrast agents on hemorrhage produced by lithotripter fields. Ultrasound Med Biol 1997;23:1435-1439.

52. Miller DL, Gies RA. Enhancement of ultrasonically induced hemolysis by perfluorocarbon-based compared to air-based echo-contrast agents. Ultrasound Med Biol 1998;24:285-295.

53. Killam AL, Greener Y, McFerran BA, Maniquis J, Bloom A, Widder KJ, Dittrich HC. Lack of bioeffects of ultrasound energy after intravenous administration of FS069 (Optison) in the anesthetized rabbit. J Ultrasound Med 1998;17:349-356.

54. Fowlkes JB, Gardner EA, Ivey JA, Carson PL. The role of acoustic radiation force in contrast enhancement techniques using bubble-based ultrasound contrast agents. J. Acoust. Soc. Am. 1993;93(4):2348.

55. Dayton PA, Morgan KE, Klibanov AL, Brandenburger GH, Nightingale KR, Ferrara KW. A preliminary evaluation of the effects of primary and secondary radiation forces on acoustic contrast agents. IEEE Trans. UFFC. 1997;44(6):1264-1277.

56. Dayton PA, Klibanov A, Brandenburger GH, Ferrara K. Acoustic radiation force in vivo: a mechanism to assist targeting of MBs. Ultrasound Med. Biol. 1999;25(8):1195-1201.

57. Lum AF, Borden MA, Dayton PA, Kruse DE, Simon SI, Ferrara KW. Ultrasound radiation force enables targeted deposition of model drug carriers loaded on MBs. J. Control. Release. 2006;111(1–2):128-134.

58. Shortencarier MJ, Dayton PA, Bloch SH, Schumann PA, Matsunaga TO, Ferrara KW. A method for radiation-force localized drug delivery using gas-filled liposome. IEEE Trans. UFFC. 2004;51(7):822-831.

59. Mesiwala AH, Farrell L, Wenzel HJ, Silbergeld DL, Crum LA, Winn HR, Mourad PD. High-intensity focused ultrasound selectively disrupts the blood-brain barrier in vivo. Ultrasound Med. Biol. 2002;28(3):389-400.

60. Seidl M, Steinbach P, Worle K, Hofstadter F. Induction of stress fibres and intercellular gaps in human vascular endothelium by shock-waves. Ultrasonics. 1994;32(5):397-400.

61. Frenkel V, Kimmel E, Iger Y. Ultrasound-facilitated transport of silver chloride

(AgCl) particles in fish skin. J. Control. Release. 2000;68(2):251-261.

62. Frenkel V, Kimmel E, Iger Y. Ultrasound-induced intercellular space widening in fish epidermis. Ultrasound Med. Biol. 2000;26(3):473-480.

63. Spengler J, Jekel M, Christensen KT. Observation and quantification of micro-particle displacements in MHz-ultrasonic standing waves. in: Proceedings of the COST-TMR Joint Meeting. 2000:18-20.

64. Ariani M, Fishbein MC, Chae JS, Sadeghi H, Michael TAD, Dubin SB, Siegel RJ. Dissolution of peripheral arterial thrombi by ultrasound. Circulation 1991;84:1680-1688.

65. Michaud LB, Valero V, Hortobagyi G. Risks and benefits of taxanes in breast and ovarian cancer. Drug Saf 2000;23:401-428.
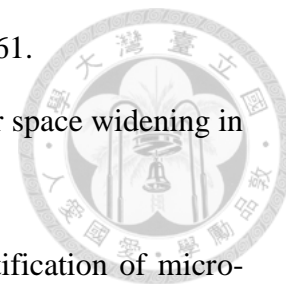
66. Ndungu JM, Lu YJ, Zhu S, Yang C, Wang X, Chen G, Shin DM, Snyder JP, Shoji M, Sun A. Targeted delivery of PTX to tumor cells: Synthesis and in vitro evaluation. J Med Chem 2010;53:3127-3132.

67. Reddy GR, Bhojani MS, McConville P, Moody J, Moffat BA, Hall DE, Kim G, Koo YE, Woolliscroft MJ, Sugai JV, Johnson TD, Philbert MA, Kopelman R, Rehemtulla A, Ross BD. Vascular targeted nanoparticles for imaging and treatment of brain tumors. Clin Cancer Res 2006;12:6677-6686.

68. Bull JL. The application of MBs for targeted drug delivery. Expert Opin Drug Deliv 2007;4:475-493.

69. Mukherjee D, Wong J, Griffin B, Ellis SG, Porter T, Sen S, Thomas JD. Ten-fold augmentation of endothelial uptake of vascular endothelial growth factor with ultrasound after systemic administration. J Am Coll Cardiol 2000;35:1678-1686.

70. Shohet RV, Chen S, Zhou YT, Wang Z, Meidell RS, Unger RH, Grayburn PA. Echocardiographic destruction of albumin MBs directs gene delivery to the myocar-

dium. Circulation 2000;101:2554-2556.

71. Taniyama Y, Tachibana K, Hiraoka K, Namba T, Yamasaki K, Hashiya N, Aoki M, Ogihara T, Yasufumi K, Morishita R. Local delivery of plasmid DNA into rat carotid artery using ultrasound. Circulation 2002;105:1233-1239.

72. Chen S, Shohet RV, Bekeredjian R, Frenkel P, Grayburn PA. Optimization of ultrasound parameters for cardiac gene delivery of adenoviral or plasmid deoxyribonucleic acid by ultrasound targeted microbubble destruction. J Am Coll Cardiol 2003;42:301-308.

73. Song J, Chappell JC, Qi M, VanGieson EJ, Kaul S, Price RJ. Influence of injection site, microvascular pressure and ultrasound variables on microbubble-mediated delivery of microspheres to muscle. J Am Coll Cardiol 2002;39:726-731.

74. Li P, Armstrong WF, Miller DL. Impact of myocardial contrast echocardiography on vascular permeability: Comparison of three different contrast agents. Ultrasound Med Biol 2004;30:83-91.
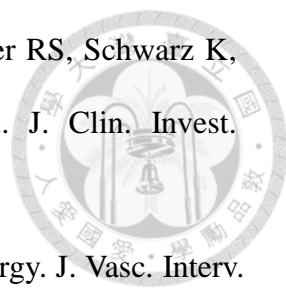
75. Kang J, Wu X, Wang Z, Ran H, Xu C, Wu J, Wang Z, Zhang Y. Antitumor effect of docetaxel-loaded lipid MBs combined with ultrasound-targeted microbubble activation on VX2 rabbit liver tumors. J Ultrasound Med 2010;29:61-70.

76. Xing W, Gang WZ, Yong Z, Yi ZY, Shan XC, Tao RH. Treatment of xenografted ovarian carcinoma using PTX-loaded ultrasound MBs. Acad Radiol 2008;15:1574-1579.

77. Tinkov S,Winter G, Coester C, Bekeredjian R. New doxorubicin-loaded phospholipid MBs for targeted tumor therapy: Part IFormulation development and in-vitro characterization. J Control Release 2010;143:143-150.

78. Kudo S. Thrombolysis with ultrasound effect. Jikeikai Med. J. 1989;104:1005-1012.
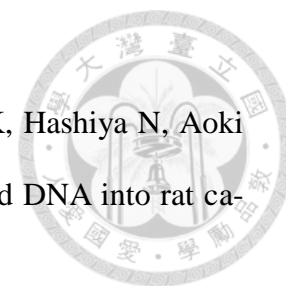
79. Francis CW, Onundarson PT, Carstensen EL, Blinc A, Meltzer RS, Schwarz K, Marder V. Enhancement of fibrinolysis in vitro by ultrasound. J. Clin. Invest. 1992;90:2063-2068.

80. Tachibana K. Enhancement of fibrinolysis with ultrasound energy. J. Vasc. Interv. Radiol. 1992;3:299-303.

81. Lauer CG, Burge R, Tang DB, Bass BG, Gomez ER, Alving BM. Effect of ultrasound on tissue-type plasminogen activator-induced thrombolysis. Circulation 1992;86:1257-1264.

82. Blinc A, Francis CW, Trudnowski JL, Carstensen EL. Characterization of ultrasound- potentiated fibrinolysis in vitro. Blood 1993;81:2636-2643.

83. Luo H, Steffen W, Cercek B, Arunasalam S, Maurer G, Siegel RJ. Enhancement of thrombolysis by external ultrasound. Am. Heart J. 1993;125:1564-1569.

84. Harpaz D, Chen X, Francis CW, Marder VJ, Metzler RS. Ultrasound enhancement of thrombolysis and reperfusion in vitro. J. Am. Coll. Cardiol. 1993;21:1507-1511.

85. Kornowski R, Meltzer R, Chernine A, Vered Z, Battler A. Does external ultrasound accelerate thrombolysis? Results from a rabbit model. Circulation 1994;89:339-344.

86. Kashyap A, Blinc A, Marder VJ, Penney DP, Francis CW. Acceleration of fibrinolysis by ultrasound in a rabbit ear model of small vessel injury. Thromb. Res. 1994;76:475-485.

87. Atar S, Luo H, Nagai T, Siegel RJ. Ultrasonic thrombolysis: catheter-delivered and transcutaneous applications. Eur. J. Ultrasound 1999;9:39-54.

88. Rosenschein U, Frimerman A, Laniado S, Miller HI. Study of the mechanism of ultrasound angioplasty from human thrombi and bovine aorta. Am. J. Cardiol.

1994;74:263-1266.

89. Steffen W, Fishbein MC, Luo H, Lee D, Nita H, Cumberland DC, Tabak SW, Carbonne M, Maurer G, Siegel RJ. High intensity, low frequency catheter-delivered ultrasound dissolution of occlusive coronary artery thrombi: an in vitro and in vivo study. J. Am. Coll. Cardiol. 1994;24:1571-1579.

90. Hamm CW, Steffen W, Terres W, de Scheerder I, Reimers, Cumberland D, Siegel RJ, Meinertz T. Intravascular therapeutic ultrasound thrombolysis in acute myocardial infarctions. Am. J. Cardiol. 1997;80:200-204.

91. Sehgal CM, Leveen RF, Shlansky-Goldberg RD. Ultrasound-assisted thrombolysis. Invest. Radiol. 1993;28:939-943.

92. Dick A, Neuerburg J, Schmitz-Rode T, Alliger H, Schmid-Schonbein, Gunther RW. Thrombolysis of mural thrombus by ultrasound: an experimental in vitro study. Invest. Radiol. 1998;33:85-90.

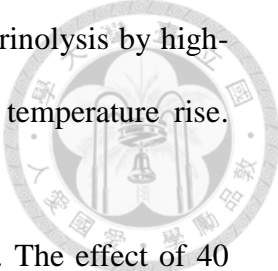93. Harpaz D, Chen X, Francis CW, Metzler RS. Ultrasound accelerates urokinase-induced thrombolysis and reperfusion. Am. Heart J. 1994;127:1211-1219.
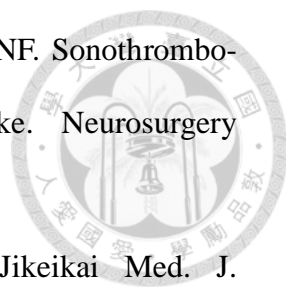
94. Datta S, McAdory LE, Tan J, Holland CK. Cavitation detection during ultrasound- assisted thrombolysis in porcine blood clots. J. Acoust. Soc. Am. 2005;117:2558.

95. Siegel RJ, Ariani M, Forester JS, Hashemi Z, DeCastro E, DonMichael TA, Fishbein MC. Cardiovascular applications of therapeutic ultrasound. J. Invas. Cardiol. 1989;4:219-229.

96. Suchkova V, Siddiqi FN, Carstensen EL, Dalecki D, Child S, Francis CW. Enhancement of fibrinolysis with 40-kHz ultrasound. Circulation 1998;98:1030-1035.

97. Suchkova VN, Carstensen EL, Francis CW. Ultrasound enhancement of fibrinolysis at frequencies of 27 to 100 kHz. Ultrasound Med. Biol. 2002;28:377-382.

98. Sakharov DV, Hekkenberg RT, Rijken DC. Acceleration of fibrinolysis by high-frequency ultrasound: the contribution of acoustic streaming and temperature rise. Thromb. Res. 2000;100:333-340.

99. Pieters M, Hekkenberg RT, Barrett-Bergshoeff M, Rijken DC. The effect of 40 kHz ultrasound on tissue plasminogen activator-induced clot lysis in three in vitro models. Ultrasound Med. Biol. 2004;30:1545-1552.

100. Bailey MR, Blackstock DT, Cleveland RO, Crum LA. Comparison of electrohydraulic lithotripters with rigid and pressure-release ellipsoidal reflectors. II. Cavitation fields. J. Acoust. Soc. Am. 1999;106:1149-1160.

101. Crum LA. Cavitation microjets as a contributory mechanism for renal calculi disintegration in ESWL. J. Urol. 1988;140:1587-1590.

102. Francis CW, Blinc A, Lee S, Cox C. Ultrasound accelerates transport of recombinant tissue plasminogen activator into clots. Ultrasound Med. Biol. 1995;21:419-424.

103. Koch S, Pohl P, Cobet U, Rainov NG. Ultrasound enhancement of liposome-mediated cell transfection is caused by cavitation effects. Ultrasound Med. Biol. 2000;26:897-903.

104. Lai CY, Wu CH, Chen CC, Li PC. Quantitative relations of acoustic inertial cavitation with sonoporation and cell viability. Ultrasound Med. Biol. 2006;32(12):1931-1941.

105. Duvshani-Eshet M, Adam D, Machluf M. The effects of albumin-coated MBs in DNA delivery mediated by therapeutic ultrasound. J. Control Release 2006;112:156-166.

106. Pfaffenberger S, Devcic-Kuhar B, Kastl S P, Huber K, Maurer G, Wojta J, Gottsauner-Wolf M. Ultrasound thrombolysis. Thromb. Haemost. 2005;94(1):26-36.

107. Medel R, Crowley RW, McKisic MS, Dumont A S, Kassell NF. Sonothrombolysis: an emerging modality for the management of stroke. Neurosurgery 2009;65(5):979-993.

108. Kudo S. Thrombolysis with ultrasound effect. Tokyo Jikeikai Med. J. 1989;104:1005-1012.

109. Tachibana K. Enhancement of fibrinolysis with ultrasound energy. J. Vasc. Interv. Radiol. 1992;3(2):299-303.

110. Lauer CG, Burge R, Tang DB, Bass BG, Gomez ER, Alving BM. Effect of ultrasound on tissue-type plasminogen activator-induced thrombolysis. Circulation. 1992;86(4):1257-1264.

111. Blinc A, Francis CW, Trudnowski JL, Carstensen EL. Characterization of ultrasound-potentiated fibrinolysis in vitro. Blood. 1993;81(10):2636-2643.

112. Luo H, Steffen W, Cercek B, Arunasalam S, Maurer G, Siegel RJ. Enhancement of thrombolysis by external ultrasound. Am. Heart J. 1993;125(6):1564-1569.

113. Harpaz D, Chen X, Francis CW, Marder VJ, Metzler RS. Ultrasound enhancement of thrombolysis and reperfusion in vitro. J. Am. Coll. Cardiol. 1993;21(6):1507-1511.

114. Chuang YH, Cheng PW, Chen SC, Ruan JL, Li PC. Effects of ultrasound-induced inertial cavitation on enzymatic thrombolysis. Ultrasonic Imaging. 2010;32(2):33-47.

115. Weller GE, Tom EM, Felix MM, Wagner WR, Villanueva FS. Multitargeting enhances adhesion of ultrasound contrast MBs to inflammatory endothelium. Circulation. 2003;108(17):516-517.

116. Weller GE, Wong MK, Modzelewski RA, Lu EX, Klibanov AL, Wagner WR, Villanueva FS. Tumor vasculature can be imaged with ultrasound contrast MBs tar-

geted via tumor-binding peptides. Circulation. 2003;108(17):515515.

117. Weller GE, Lu E, Csikari MM, Klibanov AL, Fischer D, Wagner WR, Villanueva FS. Ultrasound imaging of acute cardiac transplant rejection with MBs targeted to intercellular adhesion molecule-1. Circulation. 2003;108(2):218-224.

118. Weller GE, Wong MKK, Modzelewski RA, Lu E, Klibanov AL, Wagner WR, Villanueva FS. Ultrasonic imaging of tumor angiogenesis using contrast MBs targeted via the tumor-binding peptide arginine-arginine-leucine. Cancer Res. 2005;65(2):533-539.

119. Winter PM, Caruthers SD, Yu X, Song SK, Chen J, Miller B, Bulte JW, Robertson JD, Gaffney PJ, Wickline SA, Lanza GM. Improved molecular imaging contrast agent for detection of human thrombus. Magn. Reson. Med. 2003;50(2):411-416.

120. Ismail S, Jayaweera AR, Camarano G, Gimple LW, Powers ER, Kaul S. Relation between air-filled albumin microbubble and red blood cell rheology in the human myocardium. Influence of echocardiographic systems and chest wall attenuation. Circulation. 1996;94(3):445-451.

121. Jayaweera AR, Edwards N, Glasheen WP, Villanueva FS, Abbot RD, Kaul S. In vivo myocardial kinetics of air-filled albumin MBs during myocardial contrast echocardiography. Comparison with radiolabeled red blood cells. Circ. Res. 1994;74(6):1157-1165.

122. Lindner JR, Song J, Jayaweera AR, Sklenar J, Kaul S. Microvascular rheology of Definity MBs after intra-arterial and intravenous administration. J. Am. Soc. Echocardiogr. 2002;5(5):396-403.

123. Keller MW, Segal SS, Kaul S, Duling BR. The behavior of sonicated albumin MBs within the microcirculation: a basis for their use during myocardial contrast echocardiography. Circ. Res. 1989;65(2):458-467.

124. Villanueva FS, Jankowski RJ, Manaugh C, Wagner WR. Albumin microbubble adherence to human coronary endothelium: implications for assessment of endothelial function using myocardial contrast echocardiography. J. Am. Coll. Cardiol. 1997;30(3):689-693.

125. Porter TR, Hiser WL, Kricsfeld D, Deligonul U, Xie F, Iversen P, Radio S. Inhibition of carotid artery neointimal formation with intravenous MBs. Ultrasound Med. Biol. 2001;27(2):259-265.

126. Keller MW, Geddes L, Spotnitz W, Kaul S, Duling BR. Microcirculatory dysfunction following perfusion with hyperkalemic, hypothermic, cardioplegic solutions and blood reperfusion. Effects of adenosine. Circulation. 1991;84(6):2485-2494.

127. Doucette JW, Corl PD, Payne HM, Flynn AE, Goto M, Nassi M, Segal J. Validation of a Doppler guide wire for intravascular measurement of coronary artery flow velocity. Circulation. 1992;85(5):1899-1911.

128. Price RJ, Skyba DM, Kaul S, Skalak TC. Delivery of colloidal particles and red blood cells to tissue through microvessel ruptures created by targeted microbubble destruction with ultrasound. Circulation. 1998;98(13):1264-1267.

129. Hwang JH, Brayman AA, Reidy MA, Matula TJ, Kimmey MB, Crum LA. Vascular effects induced by combined 1-MHz ultrasound and microbubble contrast agent treatments in vivo. Ultrasound Med. Biol. 2005;31(4):553-564.

130. Devcic-Kuhar B, Pfaffenberger S, Groschl M, Kollmann C, Benes E, Gottsauner-Wolf M. In vitro thrombolysis enhanced by standing and travelling ultrasound wave fields. Ultrasound Med. Biol. 2002;28(9):1181-1187.

131. Hashizume H, Baluk P, Morikawa S, McLean JW, Thurston G, Roberge S, Jain RK, McDonald DM. Openings between defective endothelial cells explain tumor vessel leakiness. Am. J. Pathol. 2000;156(4):1363-1380.

132. Tartis MS, McCallan J, Lum AF, LaBell R, Stieger SM, Matsunaga TO, Ferrara KW. Therapeutic effects of PTX-containing ultrasound contrast agents. Ultrasound Med. Biol. 2006;32(11):1771-1780.

133. Bloch SH, Dayton PA, Ferrara KW. Targeted imaging using ultrasound contrast agents. Progress and opportunities for clinical and research applications. IEEE Eng. Med. Biol. Mag. 2004;23(5):18-29.

134. Rychak JJ, Klibanov AL, Hossack JA. Acoustic radiation force enhances targeted delivery of ultrasound contrast MBs: in vitro verification. IEEE Trans. UFFC. 2005;52(3):421-433.

135. Stephens D, Lu X, Dayton P, Kruse D, Ferrara KW. Multi-frequency array development for drug delivery therapies. in Proceedings of the IEEE Ultrasonics Symposium. 2006:66-69.

136. Zhao S, Borden M, Bloch SH, Kruse D, Ferrara KW, Dayton PA. Radiation-force assisted targeting facilitates ultrasonic molecular imaging. Mol. Imaging. 2004;3(3):135-148.

137. Coussios CC, Roy RA. Applications of acoustics and cavitation to noninvasive therapy and drug delivery. Annu Rev Fluid Mech 2008;40:395-420.

138. Datta S, Coussios CC, Ammi AY, Mast TD, de Courten-Myers GM, Holland CK. Ultrasound-enhanced thrombolysis using Definity as a cavitation nucleation agent. Ultrasound Med Biol 2008;34:1421-1433.

139. Hitchcock KE, Holland CK. Ultrasound-assisted thrombolysis for stroke therapy: better thrombus break-up with bubbles. Stroke 2010;41:S50-53.

140. Bao SP, Thrall B D, Miller DL. Transfection of a reporter plasmid into cultured cells by sonoporation in vitro. Ultrasound Med Biol 1997;23:953-959.

141. Hynynen K, McDannold N, Vykhodtseva N, Jolesz FA. Noninvasive MR imag-

ing-guided focal opening of the blood-brain barrier in rabbits. Radiology 2001;220:640-646.

142. Tachibana K, Uchida T, Ogawa K, Yamashita N, Tamura K. Induction of cell-membrane porosity by ultrasound. Lancet 1999;353:1409.

143. Amabile PG, Waugh JM, Lewis TN, Elkins CJ, Janas W, Dake MD. High-efficiency endovascular gene delivery via therapeutic ultrasound. J Am Coll Cardiol 2001;37:1975-1980.

144. Zhang SG, Duncan JH, Chahine GL. The final stage of the collapse of a cavitation bubble near a rigid wall. J Fluid Mechanics 1993;257:147-181.

145. Prentice P, Cuschierp A, Dholakia K, Prausnitz M, Campbell P. Membrane disruption by optically controlled microbubble cavitation. Nat Phys 2005;1:107-110.

146. Skyba DM, Price RJ, Linka AZ, Skalak TC, Kaul S. Direct in vivo visualization of intravascular destruction of MBs by ultrasound and its local effects on tissue. Circulation 1998;98:290-293.

147. Juffermans LJM, KampO, Dijkmans PA, Visser CA, Musters RJP. Low-intensity ultrasound-exposed MBs provoke local hyperpolarization of the cell membrane via activation of BKCa channels. Ultrasound Med Biol 2008;34:502-508.

148. Porter TR, Iversen PL, Li S, Xie F. Interaction of diagnostic ultrasound with synthetic oligonucleotide labeled perfluorocarbon-exposed sonicated dextrose albumin MBs. J Ultrasound Med 1996;15:577-584.

149. Price RJ, Skyba DM, Kaul S, Skalak TC. Delivery of colloidal particles and red blood cells to tissue through microvessel ruptures created by targeted microbubble destruction with ultrasound. Circulation 1998;98:1264-1267.

150. Main ML, Grayburn PA. Clinical applications of transpulmonary contrast echocardiography. Am Heart J 1999;137:144-153.
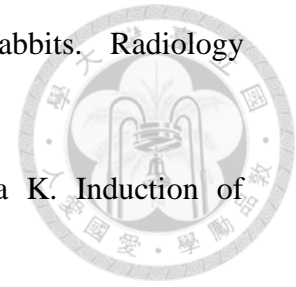
151. Takalkar AM, Klibanov AL, Rychak JJ, Lindner JR, Ley K. Binding and detachment dynamics of MBs targeted to P-selectin under controlled shear flow. J Control Release 2004;96:473-482.

152. Fritz TA, Unger EC, Sutherland G, Sahn D. Phase I clinical trials of MRX-115. A new ultrasound contrast agent. Invest Radiol 1997;32:735-740.

153. Yan F, Li X, Jin QF, Jiang CX, Zhang ZD, Ling T, Qiu BS, Zheng HR. Therapeutic ultrasonic MBs carrying PTX and Lyp-1 peptide: preparation, characterization and application to ultrasound-assisted chemotherapy in breast cancer cells Ultrasound Med Biol 2011;37:768-779.

154. Iyer AK, Khaled G, Fang J, Maeda H. Exploiting the enhanced permeability and retention effect for tumor targeting. Drug Discov Today 2006;11:812-818.
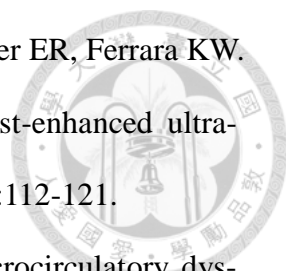
155. Seidl M, Steinbach P, Worle K, Hofstadter F. Induction of stress fibers and intercellular gaps in human vascular endothelium by shockwaves. Ultrasonics 1994;32:397-400.

156. Frenkel V, Kimmel E, Iger Y. Ultrasoundfacilitated transport of silver chloride (AgCl) particles in fish skin. J Controlled Release 2000;68:251-261.

157. Miller DL, Quddus J. Diagnostic ultrasound activation of contrast agent gas bodies induces capillary rupture in mice. Proc Natl Acad Sci U S A 2000;97:10179-10184.

158. Mesiwala AH, Farrell L, Wenzel HJ, Silbergeld DL, Crum LA, Winn HR, and Mourad PD. High-intensity focused ultrasound selectively disrupts the blood-brain barrier in vivo. Ultrasound Med. Biol. 2002;28:389-400.

159. Sheikov N, McDannold N, Vykhodtseva N, Jolesz F, Hynynen K. Cellular mechanisms of the blood-brain barrier opening induced by ultrasound in presence of MBs. Ultrasound Med Biol 2004;30:979-989.

160. Stieger SM, Caskey CF, Adamson RH, Qin S, Curry FR, Wisner ER, Ferrara KW. Enhancement of vascular permeability with lowfrequency contrast-enhanced ultrasound in the chorioallantoic membrane model. Radiology 2007;243:112-121.

161. Keller MW, Geddes L, Spotnitz W, Kaul S, Duling BR. Microcirculatory dysfunction following perfusion with hyperkalemic, hypothermic, cardioplegic solutions and blood reperfusion. Effects of adenosine. Circulation 1991;84:2485-2494.

162. Villanueva FS, Jankowski RJ, Manaugh C, Wagner WR. Albumin microbubble adherence to human coronary endothelium: implications for assessment of endothelial function using myocardial contrast echocardiography. J Am Coll Cardiol 1997;30:689-693.

163. Porter TR, Hiser WL, Kricsfeld D, Deligonui U, Xie F, Iversen P, Radio S. Inhibition of carotid artery neointimal formation with intravenous MBs. Ultrasound Med Biol 2001;27:259-265.

164. Porter TR, Knnap D, Venneri L, Oberdorfer J, Lof J, Iversen P, Radio S. Increased suppression of intracoronary c-myc protein synthesis within the stent or balloon injury site using an intravenous microbubble delivery system containing antisense to cmyc: comparison with direct intracoronary injection. J Am Coll Cardiol 2003;41:431A.

165. Tiruppathi C, Song W, Bergenfeldt M, Sass P, and Malik AB. Gp60 activation mediates albumin transcytosis in endothelial cells by tyrosine kinase-dependent pathway. J Biol Chem 1997;272:25968-25975.

166. Minshall RD, Tiruppathi C, Vogel SM, Niles WD, Gilchrist A, Hamm HE, and Malik AB. Endothelial cell-surface gp60 activates vesicle formation and trafficking via G(i)-coupled Src kinase signaling pathway. J Cell Biol 2000;150:1057-1070.

167. Ghinea N, Eskenasy M, Simionescu M, and Simionescu N. Endothelial albumin

binding proteins are membrane-associated components exposed on the cell surface. J Biol Chem 1989;264:4755-4758.

168. Simionescu M and Simionescu N. Endothelial transport of macromolecules: transcytosis and endocytosis. A look from cell biology. Cell Biol Rev 1991;25:1-78.

169. Schnitzer JE. Gp60 is an albumin-binding glycoprotein expressed by continuous endothelium involved in albumin transcytosis. Am J Physiol Heart Circ Physiol 1992;262:H246-H254.

170. Schnitzer JE and Oh P. Albondin-mediated capillary permeability to albumin. Differential role of receptors in endothelial transcytosis and endocytosis of native and modified albumins. J Biol Chem 1994;269:6072-6082.

171. Heldin CH, Miyazono K, ten Dijke P. TGF-beta signaling from cell membrane to nucleus through SMAD proteins. Nature 1997;390:465-471.

172. Itoh S, Itoh F, Goumans MJ, Ten Dijke P. Signaling of transforming growth factor-beta family members through Smad proteins. Eur J Biochem 2000;267:6954-6967.

173. Siddiqui SS, Siddiqui ZK, Malik AB. Albumin endocytosis in endothelial cells induces TGF-β receptor II signaling. Am J Physiol Lung Cell Mol Physiol 2004;286:L1016-L1026.

174. Cui W, Fowlis DJ, Bryson S, Duffie E, Ireland H, Balmain A, Akhurst RJ. TGFβ1 inhibits the formation of benign skin tumors, but enhances progression to invasive spindle carcinomas in transgenic mice. Cell 1996;86:531-542.

175. Derynck R, Akhurst RJ, Balmain A. TGF-β signaling in tumor suppression and cancer progression. Nat Genet 2001;29:117-129.

176. Schmierer B, Hill CS. TGFbeta-SMAD signal transduction: molecular specificity and functional flexibility. Nat Rev Mol Cell Biol 2007;8:970-982.

177. Teicher BA. Malignant cells, directors of the malignant process: role of trans-

forming growth factor-beta. Cancer Metastasis Rev 2001;20:133-143.

178. Sollner K, Bondy C. The mechanism of coagulation by ultrasound waves. Trans Faraday Soc 1936;32:616-623

179. Dayton PA, Morgan KE, Klibanov AL, Brandenburger G, Nightingale KR, and Ferrara KW. A preliminary evaluation of the effects of primary and secondary radiation forces on acoustic contrast agents. IEEE Trans Ultrason Ferroelectr Freq Control 1997;44:1264-1277.

180. Dayton PA, Klibanov A, Brandenburger G, Ferrara K. Acoustic radiation force in vivo: A mechanism to assist targeting of MBs. Ultrasound Med. Biol 1999;25:1195-1201.

181. Seidl M, Steinbach P, Worle K, Hofstadter F. Induction of stress fibers and intercellular gaps in human vascular endothelium by shock-waves. Ultrasonics 1994;32:397-400.

182. Shortencarier MJ, Dayton PA, Bloch SH, Schumann PA, Matsunaga TO, Ferrara KW. A method for radiation-force localized drug delivery using gas-filled liposheres. IEEE Trans Ultrason Ferroelectr Freq Control 2004;51:822-831.

183. Lum AF, Borden MA, Dayton PA, Kruse DE, Simon SI, Ferrara KW. Ultrasound radiation force enables targeted deposition of model drug carriers loaded on MBs. J Control Release 2006;111:128-134.

184. Chuang YH, Cheng PW, Li PC. Combining radiation force with cavitation for enhanced sonothrombolysis. (2013; in press).

185. Zhao S, Borden MA, Bloch SH, Kruse DE, Ferrara KW, Dayton PA. Radiation-force assisted targeting facilitates ultrasonic molecular imaging. Molec Imag 2004;3:135-148.

186. Borden MA, Sarantos MR, Stieger SM, Simon SI, Ferrara KW, Dayton P.A. Ul-

trasound radiation force modulates ligand availability on targeted contrast agents. Molec Imag 2006;5:139-147.

187. van Wamel A, Kooiman K, Harteveld M, Emmer M, ten Cate FJ, Versluis M, de Jong N. Vibrating MBs poking individual cells: drug transfer into cells via sono-poration. J Control Release 2006;112:149-155.

188. Tran TA, Roger S, Le Guennec JY, Tranquart F, Bouakaz A. Effect of ultra-sound-activated MBs on the cell electriphysiological properties. Ultrasound Med Biol 2007;33:158-163.

189. Stumm S, Meyer A, Lindner M, Bastert G, Wallwiener D, Guckel B. PTX treat-ment of breast cancer cell lines modulates Fas/Fas ligand expression and induces apoptosis which can be inhibited through the CD40 receptor. Oncology 2004;66:101-111.

190. Yan F, Li X, Jin QF, Jiang CX, Zhang ZD, Ling T, Qiu BS, Zheng HR. Thera-peutic ultrasonic MBs carrying PTX and LyP-1 peptide: preparation, characterization and application to ultrasound-assisted chemotherapy in breast cancer cells. Ultrasound Med Biol 2011;37:768-779.

List of Figures:

4×107/ml. Red arrowheads indicate the clot surface. (a) and (b) are control group. (c) and (d) are radiation force group. (e) and (f) are cavitation group. (g) and (h) are radiation force combined with cavitation group. The photographs in the same experimental group are from the same slice.
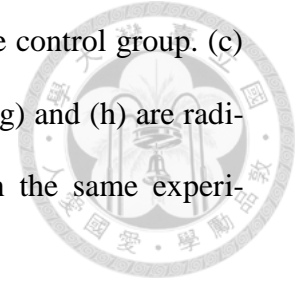
Fig. 11. Confocal microscopy photographs of blood clots. Upper and lower rows are in color and FITC fluorescence mode, respectively. Microbubble concentration is 1.6×107/ml. Red arrowheads indicate the clot surface. (a) and (b) are radiation force group. (c) and (d) are cavitation group. (e) and (f) are radiation force combined with cavitation group. The photographs in the same experimental group are from the same slice.

Fig. 12. Confocal microscopy photographs of blood clots. Upper and lower rows are in color and FITC fluorescence mode, respectively. Microbubble concentration is 8×106/ml. Red arrowheads indicate the clot surface. (a) and (b) are radiation force group. (c) and (d) are cavitation group. (e) and (f) are radiation force combined with cavitation group. The photographs in the same experimental group are from the same slice.

Fig. 13. Calculations about fluorescence intensity and distribution in depth. (a) Example fluorescence curve sampled from fluorescence images in Fig. 10, 11, 12 converted into grayscale values. The dashed line represents the calculated depth and the grayscale value used when calculating the average fluorescence intensity. (b) Average fluorescence intensity. (c) Fluorescence distribution in depth from clot surface. Data in panels b and c are mean and SD values.

Figure 14. Setup for acoustic stimulation.

Figure 15. Flow cytometry results of cell apoptosis after applying PTX-loaded MBs, an acoustic radiation force, and cavitation: (a) control, (b) albumin-shelled MBs only,

(c) PTX only, (d) PTX-loaded albumin MBs, (e) a radiation force and PTX-loaded albumin MBs, (f) cavitation and PTX-loaded albumin MBs, and (g) a radiation force, cavitation, and PTX-loaded albumin MBs.

Figure 16. Statistics results of the cell apoptosis rate from flow cytometry. The mean percentage of annexin-V-positive cells from individual experiments is shown for each condition. Error bars indicate standard deviations. RF, radiation force.

Figure 17. Microscopy images of MB–cell interactions immediately after applying a radiation force and TGF-β_1: (a) control, (b) fluorescent MBs only, (c) fluorescent MBs and a radiation force, and (d) TGF-β_1, fluorescent MBs, and a radiation force. Upper row of images are from bright-field photography, while those in the lower row are from the FITC fluorescence mode. The intensity of annexin V staining reflects the degree of apoptosis. Scale bars indicate 50 μm.

Figure 18. Microscopy images of MB–cell interactions at 24 hours after applying a radiation force and TGF-β_1: (a) control, (b) fluorescent agent (biotin-4-fluorescein) only, (c) fluorescent albumin MBs, (d) PTX-loaded fluorescent albumin MBs, (e) fluorescent albumin MBs and a radiation force, (f) TGF-β_1 and fluorescent albumin MBs, and (g) TGF-β_1, fluorescent albumin MBs, and a radiation force. Upper row of images are from bright-field photography, while those in the lower row are from the FITC fluorescence mode. The intensity of annexin V staining reflects the degree of apoptosis. Scale bars indicate 50 μm.

Figure 19. Microscopy images of fluorescent albumin MBs inside breast cancer cells for bright-field photography (left) and FITC fluorescence mode (right). Scale bars indicate 10 μm.